The Astrophysical Journal Supplement Series, 208:9 (22pp), 2013 September doi:10.1088/0067-0049/208/1/9

INTRINSIC COLORS, TEMPERATURES, AND BOLOMETRIC CORRECTIONS OF PRE-MAIN-SEQUENCE STARS

Mark J. Pecaut and Eric E. Mamajek
University of Rochester, Department of Physics and Astronomy, Rochester, NY 14627-0171, USA
Received 2012 December 14; accepted 2013 July 3; published 2013 September 4

ABSTRACT

We present an analysis of the intrinsic colors and temperatures of 5–30 Myr old pre-main-sequence (pre-MS) stars using the F0- through M9-type members of nearby, negligibly reddened groups: the η Cha cluster, the TW Hydra Association, the β Pic Moving Group, and the Tucana-Horologium Association. To check the consistency of spectral types from the literature, we estimate new spectral types for 52 nearby pre-MS stars with spectral types F3 through M4 using optical spectra taken with the SMARTS 1.5 m telescope. Combining these new types with published spectral types and photometry from the literature (Johnson–Cousins BVI_C, 2MASS JHK_S and *WISE* $W1$, $W2$, $W3$, and $W4$), we derive a new empirical spectral type–color sequence for 5–30 Myr old pre-MS stars. Colors for pre-MS stars match dwarf colors for some spectral types and colors, but for other spectral types and colors, deviations can exceed 0.3 mag. We estimate effective temperatures ($T_{\rm eff}$) and bolometric corrections (BCs) for our pre-MS star sample through comparing their photometry to synthetic photometry generated using the BT-Settl grid of model atmosphere spectra. We derive a new $T_{\rm eff}$ and BC scale for pre-MS stars, which should be a more appropriate match for T Tauri stars than often-adopted dwarf star scales. While our new $T_{\rm eff}$ scale for pre-MS stars is within $\simeq$100 K of dwarfs at a given spectral type for stars <G5, for G5 through K6, the pre-MS stars are $\sim$250 K cooler than their MS counterparts. Lastly, we present (1) a modern $T_{\rm eff}$, optical/IR color, and BC sequence for O9V-M9V MS stars based on an extensive literature survey, (2) a revised Q-method relation for dereddening *UBV* photometry of OB-type stars, and (3) introduce two candidate spectral standard stars as representatives of spectral types K8V and K9V.

Key words: open clusters and associations: individual (η Cha cluster, TW Hydra Association, β Pic Moving Group, Tucana-Horologium Association) – stars: fundamental parameters – stars: pre-main sequence

Online-only material: machine-readable tables

1. INTRODUCTION AND BACKGROUND

Knowledge of the stellar intrinsic color locus is an essential ingredient in studying young stellar populations. Recently formed stars are typically either distant, and thus outside of the "Local Bubble" of low reddening in the solar vicinity, or they are still embedded in their natal molecular cloud. Hence, we cannot assume negligible reddening and extinction for most pre-main sequence (pre-MS) stars. Interstellar reddening is conventionally estimated using tabulated intrinsic colors of dwarf field stars on the MS (e.g., Kenyon & Hartmann 1995). However, this likely introduces systematic errors in the analysis since the pre-MS stars are in a different evolutionary stage than the MS calibrators and may not exhibit "standard" dwarf colors. Accurate H-R diagram placement depends on accurate extinction and effective temperature ($T_{\rm eff}$) estimates. If the extinction or $T_{\rm eff}$ is systematically in error because of systematics in the intrinsic color and $T_{\rm eff}$ tabulations as a function of spectral type, this will obviously introduce systematic errors in the H-R diagram placement and ages and masses inferred from comparison to evolutionary tracks. For pre-MS stars, systematic errors in ages may systematically shift the inferred timescales for protoplanetary disk dissipation and giant planet formation (e.g., Mamajek 2009; Bell et al. 2013). The H-R diagram presents an opportunity for stellar theoretical evolutionary models to make contact with observations, but if our H-R diagram placement is plagued with systematic errors, this makes testing evolutionary models impossible. Thus it is imperative that the intrinsic color and $T_{\rm eff}$ scale be accurately known and as free of systematic errors as possible.

Previous studies have noted that the intrinsic colors of young stars differ from that of MS stars (e.g., Gullbring et al. 1998; Luhman 1999; Bell et al. 2012). Stauffer et al. (2003) investigated Pleiades (age $\sim$125 Myr; Stauffer et al. 1998) zero-age MS K-stars exhibiting bluer $B-V$ colors as a function of spectral type than their counterparts in Praesepe (age $\sim$750 Myr; Gáspár et al. 2009), and concluded that the effect was age-dependent. Their study identified starspots and plages as the most likely cause of the bluer $B-V$ colors and concluded that all young K dwarfs will exhibit this effect. Da Rio et al. (2010) constructed a young star intrinsic color sequence in their study of the star-formation history of Orion Nebula Cluster by merging synthetic colors interpolated to a 2 Myr isochronal surface gravity with empirical colors from Kenyon & Hartmann (1995). However, this implicitly charges the color discrepancy solely to lower surface gravity. Furthermore, synthetic near-infrared colors such as $J-H$ and $H-K_S$ do not follow observed intrinsic color sequences for M-dwarfs redder than $V-K_S \gtrsim 4.0$ (see, e.g., Casagrande et al. 2008), so we do not expect synthetic colors will accurately predict the sequences of young stars (though see also Scandariato et al. 2012). Luhman et al. (2010b, 2010a) compiled a list of the IR photospheric colors for young K4- through L0-type objects by fitting the blue envelope of the spectral-type–color-sequence of young, nearby stars from Taurus, Chamaeleon I, the η Cha cluster, the ϵ Cha cluster, and the TW Hydra Association (TWA). The Luhman et al. (2010b)

tabulation is empirically derived and thus does not depend on synthetic colors.

Here we offer an alternative and expanded pre-MS intrinsic color tabulation by including optical BVI_C colors, including earlier spectral types, and using the young stars' spectral energy distributions (SEDs) to estimate effective temperatures and construct a temperature and bolometric correction (BC) scale. In this work we examine spectral types F0 through M9.5, but our temperature scale only extends to types as late as M5. In Section 2 we describe our sample, and in Section 3 we describe the spectroscopy and photometry data used for our analysis. In Section 4 we describe our spectroscopy, the derivation of our pre-MS intrinsic colors, and the derivation of our effective temperature and BC scale for pre-MS stars. Finally, in Section 5 we compare our temperature scale and angular diameter estimates to previous results in the literature.

2. SAMPLE SELECTION

Our sample consists of members of young ($\lesssim$30 Myr), nearby moving groups including the β Pic moving group, TWA, the Tucana-Horologium moving group (Tuc-Hor), and the η Cha cluster. The members of these groups are all predominantly pre-MS (with the exception of a handful of intermediate-mass A-type stars, which we omit) and thus will allow us to study the observed color differences between MS stars and pre-MS stars. β Pic, TWA, and Tuc-Hor members are less than 75 pc distant and thus lie within the Local Bubble, within which objects are subject to negligible reddening ($E(B-V) < 0.002$, using $N_{\rm H} \lesssim 10^{19}$ cm^{-2} inside the local bubble from Cox & Reynolds 1987 and $N({\rm H\,I})/E(B-V) = 4.8 \times 10^{21}$ cm^{-2} mag^{-1} from Savage & Mathis 1979). η Cha is slightly more distant than the others ($\sim$95 pc) but also has $A_V \simeq 0$ (Mamajek et al. 1999; Luhman & Steeghs 2004). The negligible interstellar reddening for these stars allows us to use their intrinsic colors to tabulate an intrinsic color–spectral type relation for young stars in the widely used Johnson–Cousins BVI_C, Two Micron All Sky Survey (2MASS; Skrutskie et al. 2006) JHK_S photometric bands and the *Wide-field Infrared Survey Explorer* (*WISE*; Wright et al. 2010) $W1$, $W2$, $W3$, and $W4$ infrared bands at 3.4 μm, 4.6 μm, 12 μm, and 22 μm, respectively.

Our sample was assembled from group membership lists from Mamajek et al. (1999), Luhman & Steeghs (2004), Lyo et al. (2004), Song et al. (2004), Zuckerman & Song (2004), Scholz et al. (2005), Torres et al. (2006), Lépine & Simon (2009), Kiss et al. (2011), Schlieder et al. (2010), Rice et al. (2010b), Zuckerman et al. (2011), Shkolnik et al. (2011), Rodriguez et al. (2011), Schlieder et al. (2012b), and Schneider et al. (2012b). Following the Weinberger et al. (2013) and Mamajek (2005) studies, we reject TWA 22 as a member of TWA based on its discrepant space motion. However, we retain it as a member of β Pic, following Teixeira et al. (2009). In addition, based on the study of Mamajek (2005) and parallax data from Weinberger et al. (2013), stars TWA 14, TWA 15A, TWA 15B, TWA 17, TWA 18, TWA 19A, TWA 19B, and TWA 24 are likely members of the Lower Centaurus-Crux subgroup of the Scorpius-Centaurus OB association and thus may be subject to non-negligible reddening, so we exclude them from our sample. We include TWA 9 as a member of TWA, though Weinberger et al. (2013) reject it. We discuss our justification for including it in Appendix A. Our sample includes 54 members of β Pic with spectral types F0-M8, 34 members of TWA with spectral types K3-M9.5, 45 members of Tuc-Hor with spectral types F2-M2, and 15 members of η Cha with spectral types K5-M5.75.

3. DATA

3.1. Spectroscopy

Though the objects in our sample have published spectral types, they are from a variety of sources and resolutions. In order to check the consistency of spectral types in the literature, we obtain new spectral types using a grid of standards from Keenan & Yorka (1988), Keenan & McNeil (1989), Kirkpatrick et al. (1991), and Henry et al. (2002). We acquired low-resolution blue ($\sim$3700 Å–5200 Å) and red ($\sim$5600 Å–6900 Å) optical spectra from the SMARTS 1.5 m telescope in Cerro Tololo, Chile for 52 members of β Pic, TWA and η Cha. The stars chosen for spectroscopy were selected based on (1) target brightness and (2) optimizing telescope time to avoid interfering with higher priority programs. The faintest targets would require prohibitively large exposure times with the RC spectrograph on the SMARTS 1.5 m telescope to obtain useful signal-to-noise ratio for spectral classification. This spectroscopic sample includes stars down to $m_V \sim 14$ mag, with spectral types F3-M4. Observations were made in queue mode with the RC spectrograph between 2011 February and 2011 July. The blue spectra were taken with the "26/Ia" setup which consists of a grating with groove density of 600 grooves mm^{-1}, a blaze wavelength of 4450 Å, and no filter. The red spectra were taken with the "47/Ib" setup which consists of a grating with a groove density of 831 grooves mm^{-1}, a blaze wavelength 7100 Å, and a GG495 filter. Both used a slit with of 110.5 μm. The resolution for the blue and red spectra are $\sim$4.3 Å and $\sim$3.1 Å, respectively. One comparison lamp exposure, HeAr for blue spectra and Neon for red, was taken immediately before three consecutive exposures of each target. The data were reduced using the SMARTS RC Spectrograph IDL pipeline of Fred Walter (Walter et al. 2004).[1] The three images are median-combined, bias-trimmed, overscan- and bias-subtracted, and flat-fielded. The spectrum is wavelength-calibrated and, as a final step, we normalize the spectra to the continuum with a low order spline in preparation for spectral classification.

3.2. Photometry

After compiling the list of nearby $\lesssim$30 Myr old stars, we assembled the most precise photometry available from the literature, listed in Table 1. All stars in our list have counterparts in the 2MASS Point Source Catalog. A few objects are known binaries but are unresolved in the 2MASS catalog. In these cases, we retain the primary in our lists but do not include the secondary since it would be of limited use without distinct near-infrared photometry. Tuc-Hor member TYC 7065-0879-1 (K0V; Torres et al. 2006) is a 1.″8 binary, resolved in Tycho-2 (Høg et al. 2000) but unresolved in 2MASS. The 2MASS point-spread function (PSF) photometry differs significantly from the 2MASS aperture photometry (e.g., $H_{\rm PSF} - H_{\rm AP} = 0.356$ mag), presumably due to a poorly fit PSF to the unresolved binary. Thus for TYC 7065-0879-1 we adopt unresolved BVI_C optical photometry and the unresolved 2MASS aperture photometry. All other objects in our sample have 2MASS PSF photometry which agrees well with the aperture photometry (when available) and therefore we simply adopt the PSF photometry. We adopt *WISE* bands $W1$, $W2$, $W3$, and $W4$ photometry from the WISE All-Sky Point Source Catalog, centered at 3.4, 4.6, 12, and 22 μm, respectively (Wright et al. 2010). Objects saturated in $W2$

[1] http://www.astro.sunysb.edu/fwalter/SMARTS/smarts_15msched.html#RCpipeline

Table 1
Spectral Types and Optical/Near-IR Photometry for Young, Nearby, Moving Group Members

Star	Grp	2MASS	SpT	Ref.	V (mag)	$B-V$ (mag)	$V-I_C$ (mag)	Ref.	J[a] (mag)	H[a] (mag)	K_S[a] (mag)	$W1$[b] (mag)	$W2$[b] (mag)	$W3$[b] (mag)	$W4$[b] (mag)
HIP 490	TH	00055255-4145109	G0V	1	7.510 ± 0.010	0.595 ± 0.008		2, 2	6.464 ± 0.020	6.189 ± 0.023	6.117 ± 0.020	6.043 ± 0.053	6.053 ± 0.023	6.105 ± 0.015	5.975 ± 0.041
HR 9	BP	00065008-2306271	F3V	3	6.190 ± 0.010	0.386 ± 0.007		2, 2	5.451 ± 0.024	5.331 ± 0.047	5.240 ± 0.024	5.245 ± 0.072		5.234 ± 0.014	4.514 ± 0.023[c]
HIP 1113	TH	00135300-7441178	G6V	4	8.760 ± 0.010	0.752 ± 0.021	0.820 ± 0.010	2, 5, 6	7.406 ± 0.021	7.087 ± 0.029	6.962 ± 0.023	6.888 ± 0.035	6.932 ± 0.020	6.907 ± 0.015	6.954 ± 0.066[c]
HIP 1481	TH	00182612-6328389	F8/G0V	4	7.460 ± 0.010	0.537 ± 0.008		2, 2	6.462 ± 0.018	6.248 ± 0.036	6.149 ± 0.017	6.141 ± 0.048	6.102 ± 0.023	6.138 ± 0.015	5.746 ± 0.031[c]
TYC 1186-706-1	BP	00233468+2014282	K7V(e)	3	10.842 ± 0.095			5	8.138 ± 0.020	7.498 ± 0.018	7.337 ± 0.021	7.181 ± 0.028	7.200 ± 0.021	7.130 ± 0.016	6.976 ± 0.082
HIP 1910	TH	00240899-6211042	M0Ve	6	11.330 ± 0.015	1.390 ± 0.015	1.840 ± 0.020	2, 2, 2	8.385 ± 0.026	7.708 ± 0.034	7.494 ± 0.021	7.354 ± 0.026	7.306 ± 0.019	7.226 ± 0.016	7.110 ± 0.087
HIP 1993	TH	00251465-6130483	M0Ve	6	11.260 ± 0.020	1.350 ± 0.020		2, 2	8.615 ± 0.027	7.943 ± 0.040	7.749 ± 0.026	7.606 ± 0.025	7.594 ± 0.020	7.515 ± 0.016	7.505 ± 0.111
HIP 2729	TH	00345120-6154583	K5V	4	9.560 ± 0.010	1.050 ± 0.020	1.380 ± 0.010	2, 2, 6	7.337 ± 0.018	6.721 ± 0.034	6.533 ± 0.018	6.427 ± 0.044	6.443 ± 0.019	6.405 ± 0.015	6.279 ± 0.048
HIP 3556	TH	00452814-5137339	M1.5	7	11.910 ± 0.015	1.480 ± 0.015	2.180 ± 0.020	2, 2, 2	8.481 ± 0.020	7.867 ± 0.024	7.623 ± 0.027	7.509 ± 0.026	7.428 ± 0.021	7.329 ± 0.016	7.320 ± 0.107
TYC 5853-1318-1	BP	01071194-1935359	M1	8	11.457 ± 0.071			9	8.149 ± 0.020	7.473 ± 0.024	7.252 ± 0.033	7.150 ± 0.030	7.118 ± 0.019	7.047 ± 0.015	7.003 ± 0.077

Notes. Groups: (BP) β Pic Moving Group; (EC) η Cha Cluster; (TWA) TW Hydra Association; (TH) Tucana–Horologium Association.

References for Spectral Type and optical BVI_C photometry: (1) Houk 1978; (2) Perryman & ESA 1997; (3) This Work (4) Houk & Cowley 1975; (5) Converted from Tycho-2 using Mamajek et al. (2002, 2006); (6) Torres et al. 2006; (7) Hawley et al. 1996; (8) Riaz et al. 2006; (9) Gray et al. 2006; (10) Jeffries 1995; (11) Henden et al. 2012; (12) Zuckerman & Song 2004; (13) Weis 1993; (14) Vyssotsky 1956; (15) Robertson & Hamilton 1987; (16) Houk & Swift 1999; (17) Stephenson & Sanwal 1969; (18) Gray 1989; (19) Houk & Smith-Moore 1988; (20) Schlieder et al. 2012a; (21) Rice et al. 2010b; (22) Luhman & Steeghs 2004; (23) Lyo et al. 2004; (24) Lawson et al. 2001; (25) Lawson et al. 2002; (26) Stephenson 1986; (27) Reid et al. 1995; (28) Koen et al. 2010; (29) Rodriguez et al. 2011; (30) Schneider et al. 2012b; (31) Scholz et al. 2005; (32) Teixeira et al. 2008; (33) Looper et al. 2010b; (34) White & Hillenbrand 2004; (35) Barrado Y Navascués 2006; (36) Shkolnik et al. 2011; (37) Kastner et al. 2008; (38) Looper et al. 2007; (39) Song et al. 2002.

[a] JHK_S photometry from the 2MASS All-Sky Point Source Catalog (Cutri et al. 2003; Skrutskie et al. 2006).

[b] $W1$, $W2$, $W3$, $W4$ photometry from WISE All Sky Data Release (Cutri & et al. 2012).

[c] Photometry excluded due to identified infrared excess (Hutchinson et al. 1990; Megeath et al. 2005; Riaz et al. 2006; Sicilia-Aguilar et al. 2009; Rebull et al. 2008; Gautier et al. 2008; Zuckerman et al. 2011; Schneider et al. 2012a, 2012b). The binary pair HIP 10679 and HIP 10680 were studied in Rebull et al. (2008), with only HIP 10679 identified as having a 24 μm excess. However, they are separated by $\sim 14''$ and thus it is likely that the HIP 10680 $W4$ photometry is contaminated by the HIP 10679 $W4$ excess, so we exclude the HIP 10680 $W4$ photometry as well.

(This table is available in its entirety in a machine-readable form in the online journal. A portion is shown here for guidance regarding its form and content.)

Table 2
Spectral Standard Stars Used for Classification

Standard	Spectral Type	Telescope/Source	References
HD 8512	K0IIIb	SMARTS 1.5 m/Stony Brook	1
HD 3651	K0V	SMARTS 1.5 m/Stony Brook	2
HD 10476	K1V	SMARTS 1.5 m/Stony Brook	1
HD 153210	K2III	SMARTS 1.5 m/Stony Brook	1
HD 22049	K2V	SMARTS 1.5 m/Stony Brook	1
HD 16160	K3V	SMARTS 1.5 m/Stony Brook	1
α Sct	K3III	SMARTS 1.5 m/Rochester	1
TW PsA	K4Ve	SMARTS 1.5 m/Rochester	1
β Cnc	K4III Ba0.5	SMARTS 1.5 m/Rochester	1
HD 82668	K5III	SMARTS 1.5 m/Rochester	1
HD 36003	K5V	SMARTS 1.5 m/Stony Brook	1
GJ 529	K6Va	SMARTS 1.5 m/Rochester	1
GJ 673	K7V	SMARTS 1.5 m/Rochester	2
HIP 111288	K8V k	SMARTS 1.5 m/Rochester	3
HD 142574	K8IIIb	SMARTS 1.5 m/Rochester	1
HIP 3261	K9V	SMARTS 1.5 m/Stony Brook	3
GJ 701	M0.0V	SMARTS 1.5 m/Rochester	4
υ Gem	M0III	SMARTS 1.5 m/Rochester	1
GJ 229A	M1.0V	SMARTS 1.5 m/Rochester	4
ν Vir	M1III	SMARTS 1.5 m/Rochester	1
GJ 411	M2+V	SMARTS 1.5 m/Rochester	1
GJ 752A	M3-V	SMARTS 1.5 m/Rochester	1
GJ 402	M4.0V	SMARTS 1.5 m/Rochester	4
Gl 9066	M5-V	SMARTS 1.5 m/Stony Brook	1
HD 151061	M5-M5.5IIIb	SMARTS 1.5 m/Rochester	1
GJ 406	M6.0V	SMARTS 1.5 m/Rochester	4
HD 118767	M6III	SMARTS 1.5 m/Rochester	1

Note. Spectral standards for F- and G-type stars were taken from Table 2 of Pecaut et al. (2012).
References. (1) Keenan & McNeil 1989; (2) Gray et al. 2003; (3) Gray et al. 2006; (4) Henry et al. 2002.

($\lesssim$6.3 mag) exhibit a flux over-estimation bias,[2] so to avoid these biases we exclude $W2$ photometry with $W2 < 6.0$ mag. For stars with *Hipparcos* catalog entries, we adopt V and $B-V$ photometry from that catalog ESA (1997). We then fill missing $B-V$ photometry using Tycho-2 photometry (B_T, V_T) converted to Johnson $B-V$ with the conversions of Mamajek et al. (2002, 2006), resorting to the conversions in Høg et al. (2000) when $B_T - V_T > 2.0$. We adopted APASS Data Release 6 (Henden et al. 2012) BV and SACY (Torres et al. 2006) BVI_C photometry where available. Conservative estimates for SACY BVI_C photometric uncertainties obtained with the FOTRAP instrument are 0.01 mag for stars brighter than $V \sim 12$ mag (C. A. O. Torres 2012, private communication). We only adopted $B-V$ colors when $\sigma_{B-V} < 0.08$ mag. We adopted $V - I_C$ photometry from Torres et al. (2006), Lawson et al. (2001), and the *Hipparcos* catalog, when it was directly observed (value "A" in field H42), since a significant portion of the tabulated $V - I_C$ photometry in the *Hipparcos* catalog is inferred from photometry in other bands or from the spectral type of the star. Though it was available for many of our objects, we did not adopt DENIS i band photometry since it saturates at ~10.3 mag (Epchtein et al. 1997) and therefore most of our objects are too bright to have reliable DENIS i photometry.

[2] http://wise2.ipac.caltech.edu/docs/release/allsky/expsup/sec6_3c.html

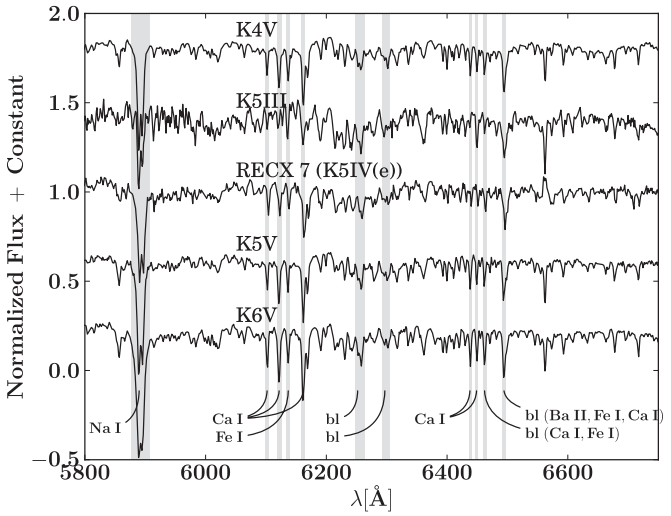

Figure 1. Spectrum of η Cha member RECX 7 (K5IV(e)) with spectral standards K4Ve (TW PsA), K5III (HD 82668), K5V (HD 36003), and K6Va (GJ 529). The primary regions used for spectral classification of K-type stars are highlighted in gray.

4. ANALYSIS

4.1. Spectral Classification

The optical spectra were visually classified by directly comparing them with spectral standards using a custom spectral software tool, *sptool*,[3] described in Pecaut et al. (2012). F- and G-type standards are taken from Table 2 of Pecaut et al. 2012; K- and M-type standards are listed in Table 2. For the blue spectra, the F-type stars were classified using the strength and profile of the Balmer lines, with particular attention to the wings of the lines in case the line depths were filled in by chromospheric emission. In addition, we use the G-band at ~4310 Å as it is a very useful temperature indicator for solar metallicity F-type stars (Gray & Corbally 2009). For G-type stars we use the G-band, Fe I lines at 4046 Å, 4325 Å, and 4383 Å, the Ca I line at 4227 Å, and the Mg Ib triplet at ~5170 Å. Spectral classification using the features described here is discussed in greater detail in Gray & Corbally (2009).

For stars with red spectra (~5600 Å–6900 Å) only, we first determine if it is a K- or M-type star based on the overall appearance of the spectrum. For K-type stars we obtain accurate spectral classifications using the Ca I lines at 6102 Å, 6122 Å, 6162 Å, and 6169 Å, the Fe I lines at 6137 Å, the relative strength of the V I and Fe I blend at 6252 Å to Ti I at 6258 Å, and the relative strength of the V, Ti, and Fe blend at 6297 Å to the Fe I blend at 6302 Å.[4] We also made use of Ca I lines at λλ6438 and 6449, the Ca I/Fe I blend at 6462 Å, the Fe I, Ti I and Cr I blend at 6362 Å, the Ba II, Fe I and Ca I blend at 6497 Å, and for the latest K-types, the TiO bands from ~6651 Å to 6852 Å. For M-type stars we use the Ca I lines at 6122 Å and 6162 Å, but predominantly rely on TiO bands from ~5847 Å to 6858 Å, ~6080 Å to 6390 Å, and ~6651 Å to 6852 Å. Following Gray et al. (2003, 2006), we assign spectral types K8 and K9, where appropriate. This is discussed in more detail in Appendix B. Example spectra with the lines used are shown in Figure 1.

While obtaining temperature types for our sample we ignored the Na I doublet at ~5889/5896 Å because it is sensitive to

[3] See http://www.pas.rochester.edu/~mpecaut/sptool or rumtph.org/pecaut/sptool/.
[4] Many of these lines were identified using the VALD service (Kupka et al. 1999), http://www.astro.uu.se/~vald/php/vald.php.

both temperature and surface gravity and is thus useful in discriminating between stars with dwarf-like, subgiant-like, or giant-like gravity. The young stars in our sample are pre-MS and thus may have an Na I doublet line similar to subgiants. Once a temperature type had been established, we compared the Na I doublet to that of a dwarf and a giant of the same temperature subclass, assigning the luminosity class "IV" if the strength was intermediate between the dwarf and giant, "IV–V" if the strength was very similar to that of a dwarf but only slightly weaker, and "V" if the Na doublet was indistinguishable from a dwarf. The results of our spectral classification are listed in Table 3.

4.2. Synthetic Colors

In order to compare observed colors to model atmosphere predictions for the color locus and the predicted effects of surface gravity, we compare our observed colors with synthetic colors calculated from the "BT-Settl" models from the Phoenix/NextGen group (Hauschildt et al. 1999; Allard et al. 2012) and the "ATLAS9" models from Castelli & Kurucz (2004). The BT-Settl models offer synthetic spectra with $400\,\mathrm{K} < T_{\rm eff} < 70000\,\mathrm{K}$, $-0.5 < \log(g) < 5.5$ and $-4.0 < [\mathrm{M/H}] < +0.5$, with α-element enhancement between +0.0 and +0.6 dex. The ATLAS9 models offer synthetic spectra with $3500\,\mathrm{K} < T_{\rm eff} < 50000\,\mathrm{K}$, $0.0 < \log(g) < 5.0$, $-5.5 < [\mathrm{M/H}] < +0.5$ with α-element enhancement between +0.0 and +0.4 dex. However, since our objects are young and are in the solar neighborhood, we assume solar metallicity with no α-element enhancement. This is consistent with the findings of Viana Almeida et al. (2009), who have spectroscopically analyzed a small sample of these young stars, obtaining $\langle[\mathrm{Fe/H}]\rangle = -0.06 \pm 0.09$ dex for a sample of nine Tuc-Hor stars and $[\mathrm{Fe/H}] = -0.13 \pm 0.08$ dex for β Pic member HD 322990. We computed synthetic colors, listed in Table 4, for solar metallicity models with $3.0 < \log(g) < 5.0$, $1400\,\mathrm{K} < T_{\rm eff} < 50000\,\mathrm{K}$ for the BT-Settl models and $3500\,\mathrm{K} < T_{\rm eff} < 50000\,\mathrm{K}$ for the ATLAS9 models, with no α-element enhancement. Pre-MS stars have lower surface gravities than MS stars at the same $T_{\rm eff}$ but both should have $3.0 < \log(g) < 5.0$. We wish to evaluate model predictions of color trends as a function of surface gravity, so we plot synthetic colors for both $\log(g) = 3.0$ and 5.0. A coeval population will have a surface gravity which varies as a function of mass, so we also plot a sequence with surface gravities given by a 20 Myr isochrone from the Baraffe et al. (1998) models. We plot commonly used colors against $V - K_S$. We chose $V - K_S$ because it is available for nearly all our objects, and it offers a very large baseline compared to other colors so it is useful as a proxy for $T_{\rm eff}$. To compute the synthetic photometry for the models, we use the updated BVI_C normalized photonic bandpasses and zero points from Bessell & Murphy (2012), including the additional zero points listed in their Table 5. To compute the 2MASS JHK_S synthetic photometry, we use the relative system response (RSR) curves available on the IPAC Web site[5] with the zero magnitude flux given in Rieke et al. (2008). Similarly, for the *WISE* bands we use RSR curves available on the IPAC Web site[6] with the zero magnitude flux given in Jarrett et al. (2011). The ATLAS9 models are sparsely sampled past ~10 μm, with only 9 points representing the flux density from 10 μm to 160 μm, so we linearly interpolate $\lambda^4 F_\lambda$ from 10 μm to 160 μm and divide by λ^4 before performing

[5] http://www.ipac.caltech.edu/2mass/releases/allsky/doc/sec6_4a.html
[6] http://wise2.ipac.caltech.edu/docs/release/prelim/expsup/sec4_3g.html

Table 3
Observations and New Spectral Types

Object	Spectral Type (This Work)	Spectral Coverage	Spectral Type (Literature)	Ref.
HR 9	F3V	Blue	F3Vn	1
TYC 1186-706-1	K7V(e)	Blue	K5	2
HIP 10679	G3V	Blue	G2V	3
HIP 10680	F7V	Blue	F7V	3
HIP 12545	K5IVe	Blue/Red	K6Ve	4
HIP 12925	F7V	Blue	F8	5
GJ 3305	M0Ve	Blue/Red	M1.1	6
V1005 Ori	K8IVe	Blue/Red	M0Ve	4
HIP 23309[b]	K8Ve	Blue/Red	K8V kee	1
HIP 23418	M4IVe	Red	M4	2
HIP 25486	F7V	Blue	F8V(n)k	1
HIP 29964	K3.5V	Blue	K3.5V ke	1
RECX 1	K5IVe	Red	K6	7
RECX 3	M3.5IV-Ve	Red	M3.25	7
RECX 4	M0IVe	Red	M1.75	7
RECX 7	K5IV(e)	Red	K6	7
RECX 10	K9IV-Ve	Red	M1	7
RECX 11	K5IVe	Red	K5.5	7
TWA 21	K3IV(e)	Red	K3Ve	4
TWA 7	M3IVe	Red	M2Ve	4
TWA 1	K8IVe	Red	K6Ve	4
TWA 2	M1.5IVe	Red	M2Ve	4
TWA 3	M4IVe	Red	M4Ve	4
TWA 12	M2IVe	Red	M2	8
TWA 4	K6IV(e)	Red	K5V	4
TWA 5A	M2IVe	Red	M2Ve	4
TWA 8A	M3IVe	Red	M3	9
TWA 9A	K7IVe	Red	K7	9
TWA 25	K9IV-Ve	Red	M1Ve	4
TWA 20	M3IVe	Red	M2	10
TWA 16	M2IVe	Red	M1.5e	11
HD 139084	G8V	Blue	K0V k	1
HD 155555AB[a]	G5V, K1V	Blue/Red	G5IV+K0IV-V	12
HD 161460	G9V	Blue	K0IV	4
HIP 88399	F4.5V	Blue/Red	F6V	4
V4046 Sgr	K4IVe	Blue	K1e	13
GSC 7396-0759	M1IVe	Red	M1Ve	4
HD 168210	G3IV	Blue	G5V	4
CD-64 1208	K4V(e)	Blue	K5Ve	4
TYC 9073-0762-1	M1Ve	Red	M1Ve	4
TYC 7408-0054-1	K8IVe	Red	K8Ve	4
TYC 6872-1011-1	K8IVe	Red	M0Ve	4
CD-26 13904	K3.5IV(e)	Red	K4V(e)	4
HIP 95270	F6V	Blue	F6V	4
TYC 7443-1102-1	K9IVe	Red	M0.0Ve	14
AT Mic A	M4IVe	Red	M4Ve	4
AT Mic B	M4IVe	Red	M4Ve	4
AU Mic	M0Ve	Red	M1Ve Ba1	15
AZ Cap	K5IVe	Red	K6Ve	4
TYC 2211-1309-1[c]	K8IVe	Red	M0.0Ve	14
CPD-72 2713	K7IVe	Red	K7Ve	4
BD-13 6424	M0V-IVe	Red	M0Ve	4

Notes.
[a] Our blue spectrum of this star was classified as G5V while our red spectrum was classified as a K1V. Therefore we adopted an overall spectral type of G5V,K1V.
[b] Our spectrum of this star did not cover the Na doublet feature.
[c] McCarthy & White (2012) were unable to detect Li in a high-resolution spectrum of this star, casting doubt on its membership in β Pic; however, we retain it as a member for the purposes of this study.

References. (1) Gray et al. 2006; (2) Stephenson 1986; (3) Harlan 1969; (4) Torres et al. 2006; (5) Cannon & Pickering 1918; (6) Shkolnik et al. 2009; (7) Luhman & Steeghs 2004; (8) Sterzik et al. 1999; (9) White & Hillenbrand 2004; (10) Reid 2003; (11) Zuckerman et al. 2001; (12) Strassmeier & Rice 2000; (13) Stephenson & Sanduleak 1977; (14) Lépine & Simon 2009; (15) Keenan & McNeil 1989.

Table 4
Synthetic Color Indices from BT-Settl and ATLAS9 Models

$T_{\rm eff}$ (K)	log(g) (dex)	$U-B$ (mag)	$B-V$ (mag)	$V-I_C$ (mag)	R_C-I_C (mag)	$J-H$ (mag)	$H-K_S$ (mag)	$V-K_S$ (mag)	$K-W1$ (mag)	$K-W2$ (mag)	$K-W3$ (mag)	$K-W4$ (mag)	$V-V_T$ (mag)	B_T-V_T (mag)	$V-H_{\rm p}$ (mag)	Model
1400	3.5	3.475	3.191	5.213	2.454	1.916	1.344	13.151	1.379	1.967	2.652	2.921	−0.405	3.747	0.979	BT-Settl
1400	4.0	4.909	0.795	7.250	2.854	1.149	0.635	13.788	0.983	1.083	2.226	2.292	0.091	1.668	2.550	BT-Settl
1400	4.5	4.959	−0.165	7.918	3.184	0.919	0.306	13.929	0.923	1.148	2.326	2.426	0.561	1.123	2.903	BT-Settl
1400	5.0	4.957	−0.945	8.421	3.433	0.893	0.098	14.184	0.873	1.363	2.474	2.631	1.085	0.836	3.189	BT-Settl
1500	3.5	3.642	3.306	5.223	2.433	1.467	1.048	12.157	1.088	1.594	2.323	2.577	−0.412	3.929	1.006	BT-Settl

Notes. All synthetic colors are computed using solar metallicity models. The BT-Settl model colors presented here adopt the Asplund et al. (2009) solar composition, whereas the ATLAS9 model colors presented here adopt the Grevesse & Sauval (1998) solar composition.

(This table is available in its entirety in a machine-readable form in the online journal. A portion is shown here for guidance regarding its form and content.)

synthetic photometry. This is not necessary for the BT-Settl models because they are sampled at 0.2 Å spectral resolution for $\lambda > 5.2\,\mu$m. The BT-Settl models shown adopt the Asplund et al. (2009) solar abundances while the ATLAS9 models shown use the Grevesse & Sauval (1998) solar abundances. The computed synthetic colors are listed in Table 4.

4.3. Empirical Colors of Dwarfs versus Pre-MS Stars

To compare dwarfs colors with pre-MS colors, we plot color–color diagrams for the young stars listed in Table 1. Figures 2 and 3 show $V-K_S$ versus $B-V$, $V-I_C$, $J-H$, $H-K_S$, K_S-W1, K_S-W2, K_S-W3, and K_S-W4 for the young stars along with the dwarf sequence described in Appendix C (listed in Table 5) and the empirical giant sequence for $B-V$ from Alonso et al. (1999) and for $V-I_C$, $J-H$, and $H-K_S$ from Bessell & Brett (1988) converted to the 2MASS photometric system with the conversions of Carpenter (2001). For reference we include the BVI_C solar colors estimated by Ramírez et al. (2012) and 2MASS JHK_S and *WISE* $W1$ $W2$ $W3$ $W4$ solar colors estimated by Casagrande et al. (2012).

Color–color plots $V-K_S$ versus $B-V$ and $V-K_S$ versus $J-H$ show the largest color difference between our young stars and the dwarf locus. Redward of $V-K_S \sim 2.0$ mag, young stars are bluer in $B-V$ than the dwarf locus, and for $V-K_S \geqslant 4.0$ they are well-matched by the 20 Myr isochronal colors. Models predict the $B-V$ colors are bluer at lower surface gravity at a given $V-K_S$, consistent with our observations, though the agreement is not perfect. Models predict little sensitivity to surface gravity for $V-K_S$ versus $V-I_C$, consistent with the location of the dwarf and giant locus as well as the placement of the young stars. For $V-K_S$ versus $J-H$ locus, a bifurcation between the dwarf and giant empirical locus occurs at $V-K_S \sim 3$ mag, which corresponds to spectral type ∼K5. This color split has been explained by the models as an effect of surface gravity, due to the CO and H_2O bands and H^- opacity (Jorgensen 1996). The young stars in our sample have surface gravities intermediate between that of the giants and dwarfs, and as a result they populate the region between the dwarf and giant loci. For $V-K_S \leqslant 3.5$, the young stars lie above the dwarf locus for colors $H-K_S$ and K_S-W1, indicating that these two colors are redder for young stars at a given $V-K_S$. We exclude photometry for objects which have previously identified infrared excesses in that respective infrared band, likely due to a dusty circumstellar disk. Excluded photometry is indicated in Table 1.

4.4. Spectral Type–Color Sequence

To define the intrinsic color sequence empirically, with the constraint of satisfying the color–color plots, we first fit a spline to spectral type versus $V-K_S$ and spectral type versus $V-I_C$. We then verify that these relations provide a good fit to the $V-K_S$ versus $V-I_C$ color–color relation as well. We then fit splines to $V-K_S$ versus $J-H$ and $V-K_S$ versus $H-K_S$ and use our spectral type–$V-K_S$ relation to anchor $J-H$ and $H-K_S$ to spectral type. Finally, we fit splines to spectral type versus color for the colors $B-V$, K_S-W1, K_S-W2, K_S-W3, and K_S-W4. $V-I_C$ data is sparse for types earlier than G5, but appears consistent with the dwarf sequence, so we simply adopt the dwarf $V-I_C$ sequence for spectral types F0 through G5 discussed in Appendix C. In Figure 4 we see that pre-MS stars later than K3 become *bluer* in $B-V$ than their MS counterparts, while those hotter than K2 are nearly indistinguishable from MS stars. Figure 4 also shows that young stars G5 and later have redder $V-K_S$ and $J-H$ colors than field dwarfs, while those earlier than G5 have $V-K_S$ and $J-H$ colors indistinguishable from field dwarfs. Pre-MS stars have $H-K_S$ colors redder than field dwarfs between spectral types F0 and M2, shown in Figure 4. The spectral type sequence for K_S-W1, K_S-W2, K_S-W3, and K_S-W4 (Figures 4 and 5) show larger scatter than for the previously discussed colors, and greater care must be taken to exclude those stars with a color excess due to the presence of a circumstellar disk. We have excluded photometry for objects with infrared excesses flagged in Table 1. AG Tri was discussed in Rebull et al. (2008) as having a possible MIPS 24 μm excess. We find that it has a K_S-W4 color excess 4.5σ above the young color sequence. We also identify HD 160305 and CD-54 7336 as having a K_S-W4 color excess at 2.9σ and 5.4σ above the young color sequence, so we also exclude them from the K_S-W4 fit. Our pre-MS intrinsic color sequence is listed in Table 6.

For some spectral type and color combinations, extinction estimates using these intrinsic colors will give different results than those which adopt dwarf colors. For example, a typical unreddened pre-MS K0 star has a $V-K_S$ color 0.24 mag redder than an MS K0. If one estimated A_V based on the stars $E(V-K_S)$ calculated using dwarf colors, then this star would appear to have $A_V = 1.12E(V-K_S) \simeq 0.27$ mag of artificial extinction, based on the apparent $V-K_S$ color difference between pre-MS and an MS K0 stars (assuming a standard $R_V = 3.1$ reddening law). A 0.3 mag systematic shift in H-R diagram placement would cause a 15 Myr old K-type star to erroneously appear 10 Myr old.

4.5. Temperature Scale

4.5.1. Technique

The effective temperature ($T_{\rm eff}$) scale for giants (e.g., van Belle et al. 1999) as a function of spectral type is ∼700–400 K

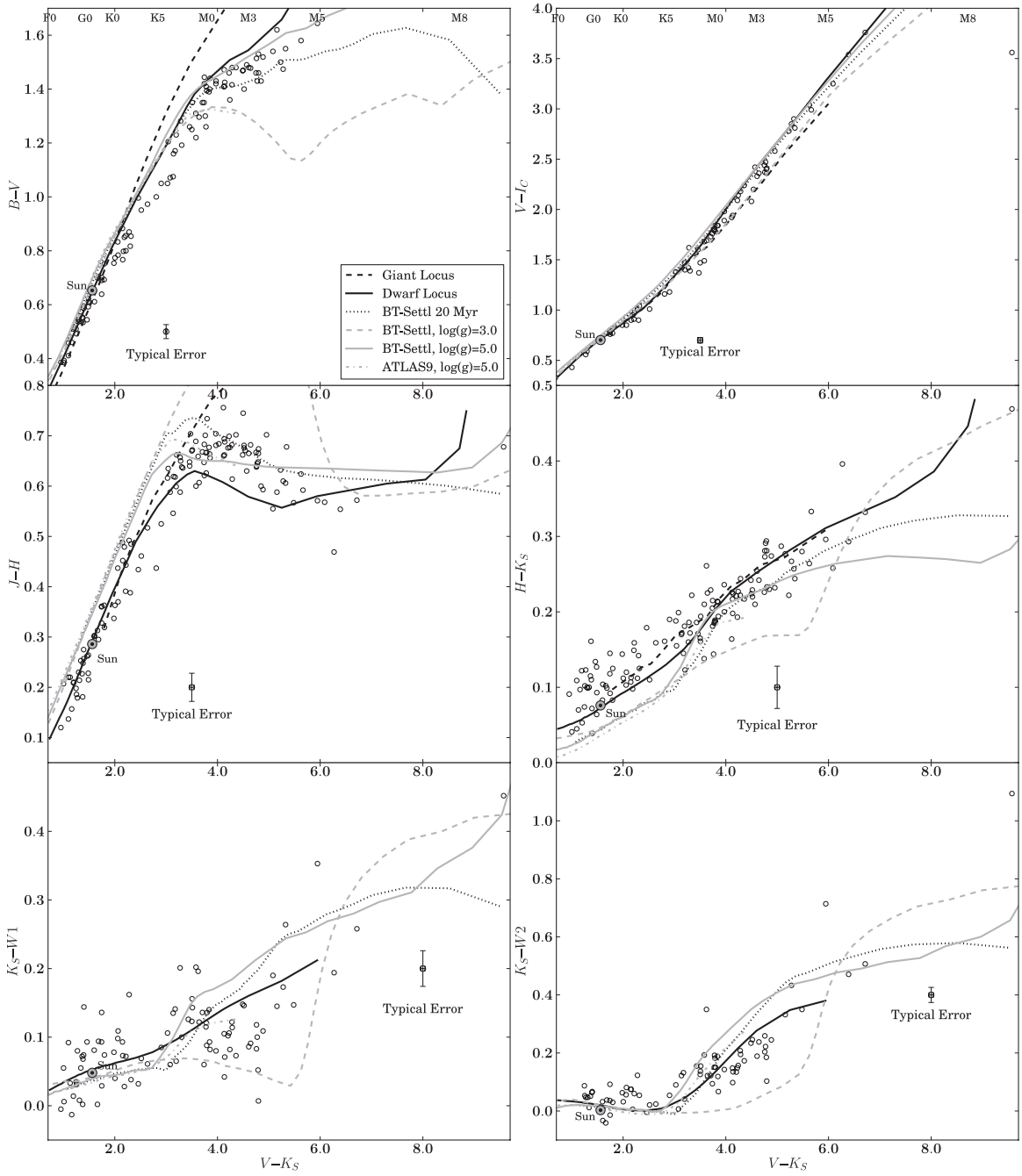

Figure 2. Comparison of $B-V$, $V-I_C$, $J-H$, $H-K_S$, K_S-W1, and K_S-W2 vs. $V-K_S$ of young stars from β Pic, η Cha, TWA, and Tuc-Hor moving groups (circles) with the dwarf color locus described in Appendix C and the giant color locus from Bessell & Brett (1988), except the $B-V$ giant locus, which is from Alonso et al. (1999). Spectral types corresponding to the $V-K_S$ colors of dwarfs are plotted along the top. Objects with a known near-IR or IR excess have been excluded (see Table 1).

cooler than dwarfs for spectral types G8 through K5, whereas M0 through M9 giants are ∼100–400 K hotter than dwarfs. Since pre-MS stars have surface gravities intermediate between dwarfs and giants, we expect that a pre-MS $T_{\rm eff}$ scale will be intermediate between dwarfs and giants (e.g., Luhman et al. 2003).

All $T_{\rm eff}$ scales depend on models (e.g., atmospheric models, limb-darkening models) to some degree. Arguably, the least model-dependent methods are those *direct* methods based on the angular diameter of the star, measured interferometrically or by lunar occultation methods. While some of the stars in our sample are candidates for angular diameter measurements (see McCarthy & White 2012), only two have actual measurements in the literature (HR 9 and 51 Eri; Simon & Schaefer 2011; see Section 5 for details). There are also *indirect* methods, such as the infrared flux method (IRFM), performed by Alonso et al. (1999), and more recently for M-dwarfs by Casagrande et al. (2008), or directly fitting SEDs to synthetic model photometry, as described by Masana et al. (2006).

Spectroscopically, young stars have been shown to exhibit more than one photospheric $T_{\rm eff}$ (Gullbring et al. 1998; Stauffer et al. 2003), so fitting synthetic spectra to observed spectra will yield a different $T_{\rm eff}$ depending on the spectral region selected for fitting. An example of this is TW Hydra, which has been

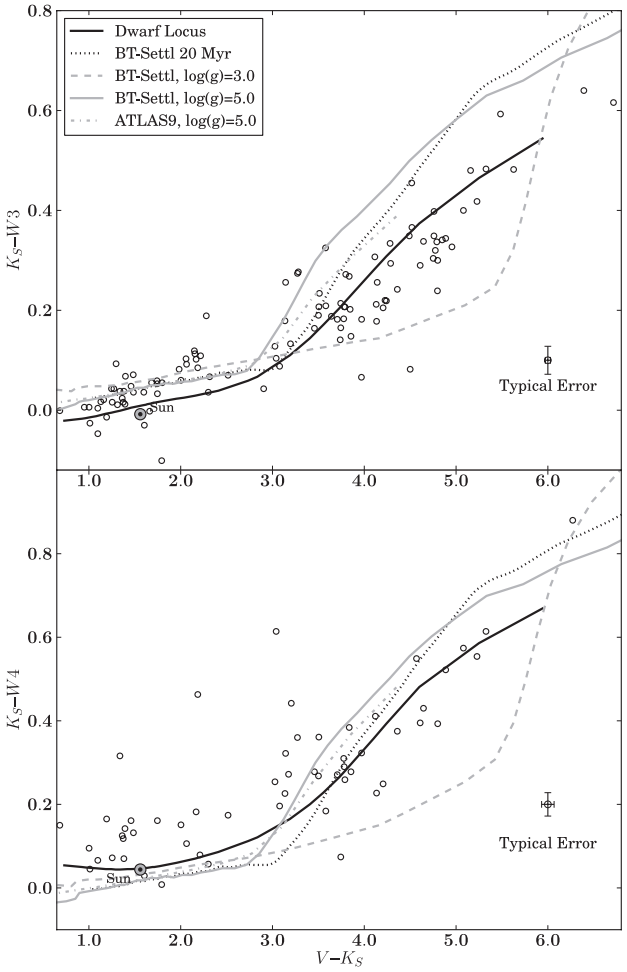

Figure 3. Same as Figure 2, except $V - K_S$ vs. $K_S - W3$ and $K_S - W4$.

consistently typed as a late K star based on optical spectra (K7e, de la Reza et al. 1989; K6e, Hoff et al. 1998; K6Ve, Torres et al. 2006; K8IVe, this work) but near-IR spectroscopy indicate a spectral type of M2.5V (Vacca & Sandell 2011). We need a method to infer temperatures that will simultaneously take into account the observed optical–IR photometry. Therefore we attempt to infer the effective temperatures by simultaneously fitting the observed photometry to synthetic models (the Spectral Energy Distribution Fitting (SEDF) method, see Masana et al. 2006). The downside of this method is that we are using models which do not completely correctly predict the colors of young stars. However, since the $T_{\rm eff}$ is *defined* by the integrated SED and the stellar radius, the observed photometry is the most direct link to the effective temperature of objects in our sample. We closely follow the formalism and methods of Masana et al. (2006) and fit the observed photometry to models by minimizing χ^2, defined as

$$\chi^2 = \sum_i \left(\frac{m_i - m_{i,\rm syn} - \mathcal{A}}{\sigma_{m_i}} \right)^2 .$$

With $m_i = B$, V, I_C, J, H, K_S, $W1$, $W2$, $W3$, and $W4$ being the observed photometry, $m_{i,\rm syn} = B_{\rm syn}$, $V_{\rm syn}$, $I_{C\,\rm syn}$, $J_{\rm syn}$, $H_{\rm syn}$, $K_{S\,\rm syn}$, $W1_{\rm syn}$, $W2_{\rm syn}$, $W3_{\rm syn}$, and $W4_{\rm syn}$ are the synthetic apparent magnitudes at the stellar surface, and $\mathcal{A}$ is the magnitude difference between the flux observed on Earth (obs) and the theoretical flux at the surface of the star (surface)[7]:

$$\mathcal{A} = -2.5 \log(F_{\rm surface}/F_{\rm obs})$$

related to the angular semi-diameter:

$$\theta = \frac{R}{d} = 10^{-0.2\mathcal{A}}.$$

We fit the observed photometry to synthetic photometry from two different libraries of synthetic spectra: the BT-Settl models[8] of Allard et al. (2012) with the Asplund et al. (2009) solar composition and the ATLAS9 models[9] of Castelli & Kurucz (2004) with the Grevesse & Sauval (1998) solar composition. The differences in the solar composition are particularly important for low-mass stars and brown dwarfs, due to the importance of TiO and VO in their spectra. The solar oxygen abundance was revised downward by 38% by Asplund et al. (2009) compared to the Grevesse & Sauval (1998) oxygen abundances. Another major difference between the ATLAS9 models and the BT-Settl models is the treatment of line opacities. The ATLAS9 models include opacity distribution functions to account for line blanketing, whereas the BT-Settl models are generated by the PHOENIX code in which the individual contribution of atoms and molecules is directly sampled over all computed points in the spectrum (Hauschildt et al. 1997). Given that the BT-Settl models offer continuity in our ability to model SEDs of F-type down to M-type stars, and the recent successes the BT-Settl models have had fitting NIR colors of low-mass stars down to ~3000 K (Allard et al. 2012), we adopt the temperatures derived from the BT-Settl models with the Asplund et al. (2009) abundances, but include the results from the ATLAS9 models to demonstrate the size of the systematic differences resulting from the assumed solar composition or model implementation.

4.5.2. Testing Technique on Objects with Measured Angular Diameters

As a reliability check for the usefulness of our method, we use the estimated solar BVI_C colors from Ramírez et al. (2012) together with the solar 2MASS JHK and *WISE* $W1$, $W2$, $W3$ and $W4$ colors from Casagrande et al. (2012) to estimate the solar $T_{\rm eff}$, assuming $\log(g) = 4.44$ and adopting the apparent V band magnitude of -26.74 ± 0.02 mag (Mamajek 2012). With these ten bands, the BT-Settl models SEDF method gives $T_{\rm eff\odot} = 5776 \pm 22$ K (remarkably within 4 K of the modern solar $T_{\rm eff}$ of 5771.8 ± 0.7 K; Mamajek 2012), and an angular diameter of $1949'' \pm 7''$. The ATLAS9 models give $T_{\rm eff\odot} = 5737 \pm 21$ K, 35 K too low but still within 2σ, and an angular diameter of $1953'' \pm 7''$. Both angular diameter measurements are systematically higher than the $1918''.3 \pm 0''.3$ angular diameter implied by the solar radius estimate of Haberreiter et al. (2008), which strongly suggests that our adopted $V_\odot$ is too high. If we instead adopt $V_\odot \equiv -26.71 \pm 0.02$ mag, we obtain angular diameters with the SEDF method of $1922'' \pm 7''$ and $1926'' \pm 7''$ with the BT-Settl and ATLAS9 models, respectively, consistent with the modern solar angular diameter estimates. Thus for consistency with the solar values, also consistent

[7] This flux is the unresolved flux integrated over the disk of the star and does not represent the resolved flux one would observe if placed on the stellar surface. The flux we are referring to is the counterpart to the apparent magnitude at the stellar surface (e.g., $B_{\rm syn}$).
[8] http://phoenix.ens-lyon.fr/Grids/BT-Settl/AGSS2009/
[9] http://wwwuser.oat.ts.astro.it/castelli/grids.html

Table 5
Intrinsic Colors of O9-M9 Dwarfs and Adopted $T_{\rm eff}$, Bolometric Correction Values

SpT	$T_{\rm eff}$ (K)	BC_V (mag)	$U-B$ (mag)	$B-V$ (mag)	$V-R_C$ (mag)	$V-I_C$ (mag)	$V-J$ (mag)	$V-H$ (mag)	$V-K_S$ (mag)	$K-W1$ (mag)	$K-W2$ (mag)	$K-W3$ (mag)	$K-W4$ (mag)
O9V	34000	−3.20	−1.114	−0.318	...	−0.369	−0.765	−0.929	−1.000	...	...	...	...
O9.5V	32000	−3.06	−1.087	−0.312	...	−0.361	−0.747	−0.908	−0.977	...	...	...	...
B0V	31500	−3.03	−1.067	−0.307	...	−0.355	−0.732	−0.891	−0.958	...	...	...	...
B0.5V	29000	−2.87	−1.026	−0.295	...	−0.338	−0.697	−0.850	−0.913	...	...	...	...
B1V	26000	−2.61	−0.995	−0.278	−0.115	−0.325	−0.667	−0.815	−0.874	...	...	...	...
B1.5V	24800	−2.43	−0.910	−0.252	−0.114	−0.281	−0.573	−0.705	−0.752	...	...	...	...
B2V	20600	−2.06	−0.790	−0.210	−0.094	−0.230	−0.457	−0.570	−0.602	...	...	...	...
B2.5V	18500	−1.79	−0.732	−0.198	−0.087	−0.210	−0.413	−0.518	−0.544	...	...	...	...
B3V	17000	−1.58	−0.673	−0.178	−0.080	−0.192	−0.373	−0.471	−0.492	...	...	...	...
B4V	16700	−1.53	−0.619	−0.165	−0.074	−0.176	−0.339	−0.431	−0.447	...	...	...	...
B5V	15700	−1.37	−0.581	−0.156	−0.070	−0.165	−0.315	−0.404	−0.417	...	...	...	...
B6V	14500	−1.16	−0.504	−0.140	−0.062	−0.145	−0.270	−0.351	−0.358	...	...	...	...
B7V	14000	−1.07	−0.459	−0.128	−0.058	−0.133	−0.244	−0.321	−0.325	...	...	...	...
B8V	12500	−0.79	−0.364	−0.109	−0.048	−0.108	−0.190	−0.257	−0.254	...	...	...	...
B9V	10700	−0.44	−0.200	−0.070	−0.028	−0.061	−0.087	−0.137	−0.121	...	...	...	...
B9.5V	10400	−0.38	−0.130	−0.050	−0.017	−0.035	−0.025	−0.069	−0.048	...	...	...	...
A0V	9700	−0.24	−0.005	0.000	0.001	0.004	0.045	0.013	0.041	...	...	...	...
A1V	9200	−0.15	0.033	0.043	0.019	0.044	0.094	0.070	0.101	...	...	...	...
A2V	8840	−0.10	0.063	0.074	0.042	0.091	0.164	0.154	0.188	...	...	...	...
A3V	8550	−0.06	0.077	0.090	0.050	0.108	0.196	0.194	0.228	...	...	...	...
A4V	8270	−0.04	0.097	0.140	0.078	0.164	0.294	0.316	0.353	...	...	...	...
A5V	8080	−0.03	0.100	0.160	0.089	0.186	0.334	0.365	0.403	...	...	...	...
A6V	8000	−0.02	0.098	0.170	0.094	0.197	0.354	0.390	0.428	...	...	...	...
A7V	7800	0.00	0.091	0.210	0.117	0.242	0.433	0.488	0.528	...	...	...	...
A8V	7500	0.00	0.082	0.250	0.140	0.288	0.509	0.584	0.626	...	...	...	...
A9V	7440	0.00	0.080	0.255	0.143	0.294	0.517	0.595	0.638	...	...	...	...
F0V	7200	−0.01	0.053	0.294	0.166	0.339	0.589	0.687	0.732	0.023	0.037	−0.021	0.054
F1V	7030	−0.01	0.021	0.334	0.190	0.385	0.662	0.781	0.828	0.027	0.036	−0.019	0.052
F2V	6810	−0.02	−0.008	0.374	0.213	0.432	0.735	0.875	0.925	0.031	0.034	−0.017	0.050
F3V	6720	−0.03	−0.016	0.389	0.222	0.449	0.763	0.910	0.961	0.032	0.034	−0.016	0.049
F4V	6640	−0.04	−0.026	0.412	0.236	0.476	0.806	0.965	1.017	0.035	0.033	−0.014	0.048
F5V	6510	−0.04	−0.029	0.438	0.252	0.506	0.852	1.025	1.079	0.037	0.032	−0.012	0.047
F6V	6340	−0.05	−0.021	0.484	0.276	0.553	0.929	1.128	1.185	0.041	0.030	−0.007	0.045
F7V	6240	−0.06	−0.012	0.510	0.290	0.579	0.971	1.184	1.244	0.043	0.028	−0.005	0.045
F8V	6150	−0.07	0.001	0.530	0.300	0.599	1.004	1.229	1.290	0.045	0.027	−0.003	0.044
F9V	6040	−0.08	0.014	0.552	0.312	0.620	1.040	1.277	1.340	0.046	0.026	−0.001	0.044
G0V	5920	−0.09	0.049	0.588	0.331	0.656	1.097	1.355	1.421	0.049	0.024	0.003	0.045
G1V	5880	−0.10	0.067	0.604	0.340	0.672	1.123	1.390	1.458	0.050	0.023	0.005	0.045
G2V	5770	−0.11	0.133	0.650	0.363	0.713	1.197	1.491	1.564	0.053	0.020	0.009	0.046
G3V	5720	−0.12	0.152	0.661	0.368	0.722	1.217	1.516	1.590	0.053	0.019	0.010	0.047
G4V	5680	−0.13	0.175	0.674	0.374	0.733	1.239	1.546	1.621	0.054	0.018	0.011	0.048
G5V	5660	−0.13	0.185	0.680	0.377	0.738	1.249	1.559	1.635	0.055	0.017	0.012	0.048
G6V	5590	−0.15	0.229	0.704	0.388	0.758	1.288	1.612	1.691	0.056	0.016	0.014	0.050
G7V	5530	−0.16	0.243	0.713	0.393	0.766	1.303	1.632	1.712	0.056	0.015	0.015	0.050
G8V	5490	−0.17	0.284	0.737	0.404	0.786	1.344	1.686	1.768	0.058	0.013	0.017	0.052
G9V	5340	−0.21	0.358	0.777	0.423	0.820	1.409	1.774	1.861	0.059	0.010	0.020	0.056
K0V	5280	−0.22	0.436	0.816	0.443	0.853	1.475	1.862	1.953	0.061	0.007	0.023	0.060
K1V	5170	−0.26	0.502	0.847	0.460	0.883	1.535	1.940	2.034	0.063	0.005	0.025	0.064
K2V	5040	−0.29	0.600	0.893	0.487	0.929	1.624	2.056	2.155	0.065	0.003	0.029	0.070
K3V	4840	−0.41	0.801	0.990	0.544	1.025	1.810	2.300	2.410	0.070	0.001	0.039	0.086
K4V	4620	−0.55	1.004	1.100	0.640	1.190	2.064	2.608	2.733	0.078	0.008	0.059	0.112
K5V	4450	−0.67	1.056	1.134	0.671	1.246	2.145	2.705	2.835	0.082	0.014	0.067	0.121
K6V	4200	−0.86	1.199	1.257	0.771	1.448	2.434	3.039	3.190	0.096	0.044	0.110	0.165
K7V	4050	−1.00	1.222	1.336	0.824	1.574	2.616	3.239	3.407	0.106	0.072	0.144	0.200
K8V	3970	−1.11	1.213	1.382	0.859	1.671	2.743	3.373	3.554	0.113	0.094	0.171	0.228
K9V	3880	−1.25	1.198	1.418	0.900	1.802	2.907	3.531	3.728	0.122	0.123	0.204	0.265
M0V	3850	−1.30	1.190	1.431	0.913	1.848	2.965	3.587	3.790	0.125	0.134	0.217	0.280
M1V	3680	−1.53	1.171	1.484	0.974	2.074	3.265	3.873	4.100	0.140	0.191	0.280	0.357
M2V	3550	−1.65	1.170	1.500	1.001	2.173	3.406	4.006	4.240	0.146	0.217	0.308	0.393
M3V	3400	−1.97	1.181	1.544	1.079	2.420	3.769	4.348	4.600	0.160	0.277	0.374	0.481
M4V	3200	−2.59	1.215	1.661	1.241	2.831	4.411	4.968	5.250	0.182	0.348	0.465	0.586
M5V	3050	−3.28	1.433	1.874	1.446	3.277	5.051	5.631	5.942	0.212	0.380	0.544	0.669
M6V	2800	−4.36	...	2.000	1.950	4.100	6.343	6.948	7.300	...	...	...	...
M7V	2650	−5.06	...	2.060	2.180	4.520	7.054	7.667	8.050	...	...	...	...
M8V	2570	−5.66	...	2.130	2.150	4.600	7.593	8.268	8.700	...	...	...	...
M9V	2450	−5.73	...	...	1.890	4.370	7.617	8.366	8.850	...	...	...	...

(This table is also available in a machine-readable form in the online journal.)

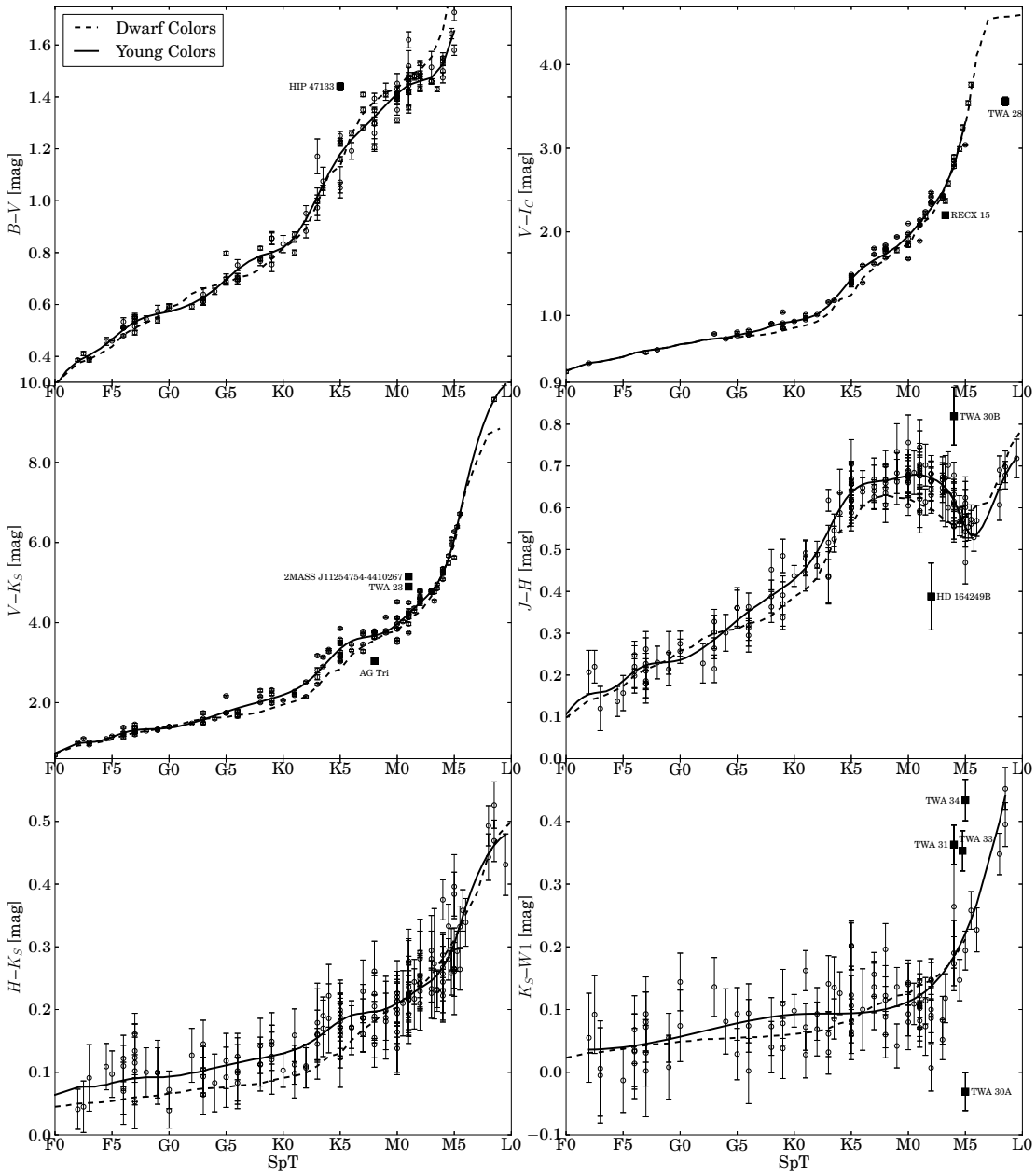

Figure 4. Comparison of $B-V$, $V-I_C$, $V-K_S$, $J-H$, $H-K_S$, and K_S-W1 of young stars from β Pic, η Cha, TWA, and Tuc-Hor moving groups (circles) with the dwarf color sequence described in this work (dashed line). The outliers (filled squares) were excluded from the fit.

with the Engelke et al. (2010) synthetic solar $V_\odot$, we adopt $V_\odot = -26.71 \pm 0.02$ mag.[10]

We also check our technique on nearby K- and M-type field dwarfs with directly measured angular diameters from the recent work of Boyajian et al. (2012b). We use photometry from Table 7 of Boyajian et al. (2012b), converting Johnson *I* to the Cousins system using the conversions in Bessell (1979) and converting Johnson *JHK* to the 2MASS system using the conversions of Carpenter (2001). We adopt *WISE* $W1$, $W3$, and $W4$ photometry with contamination and confusion flags "0" from the WISE All Sky Point Source Catalog. Following Boyajian et al. (2012b), we adopted $\log(g) = 4.5$ and the metallicity appropriate for each system. We adopt uncertainties of $\sigma_{\log(g)} = 0.2$ dex and $\sigma_{[m/H]} = 0.1$ dex. Our SEDF-derived $T_{\rm eff}$ for these stars are listed in Table 7, and plotted with the Boyajian et al. (2012b) $T_{\rm eff}$ values in Figure 10. The mean difference between our SEDF-derived $T_{\rm eff}$ values and those based on angular diameter measurements from Boyajian et al. (2012b) is 13 K with a 1σ dispersion of 108 K. We conclude that our technique works well for the Sun and nearby dwarfs with angular diameter measurements, and gives us some confidence that this method will accurately predict the effective temperatures of our pre-MS stars.

[10] $V_\odot = -26.71 \pm 0.02$ mag implies that $M_{V,\odot} = 4.862 \pm 0.020$ mag. Based on the IAU scale the solar luminosity estimate of Mamajek (2012) ($3.8270 \pm 0.0014 \times 10^{33}$ erg s^{-1}) leads to $M_{\rm bol,\odot} = 4.7554 \pm 0.0004$ mag, $BC_{V,\odot} = -0.107 \pm 0.02$ mag. A summary of solar *V* magnitude estimates is available at https://sites.google.com/site/mamajeksstarnotes/basic-astronomical-data-for-the-sun.

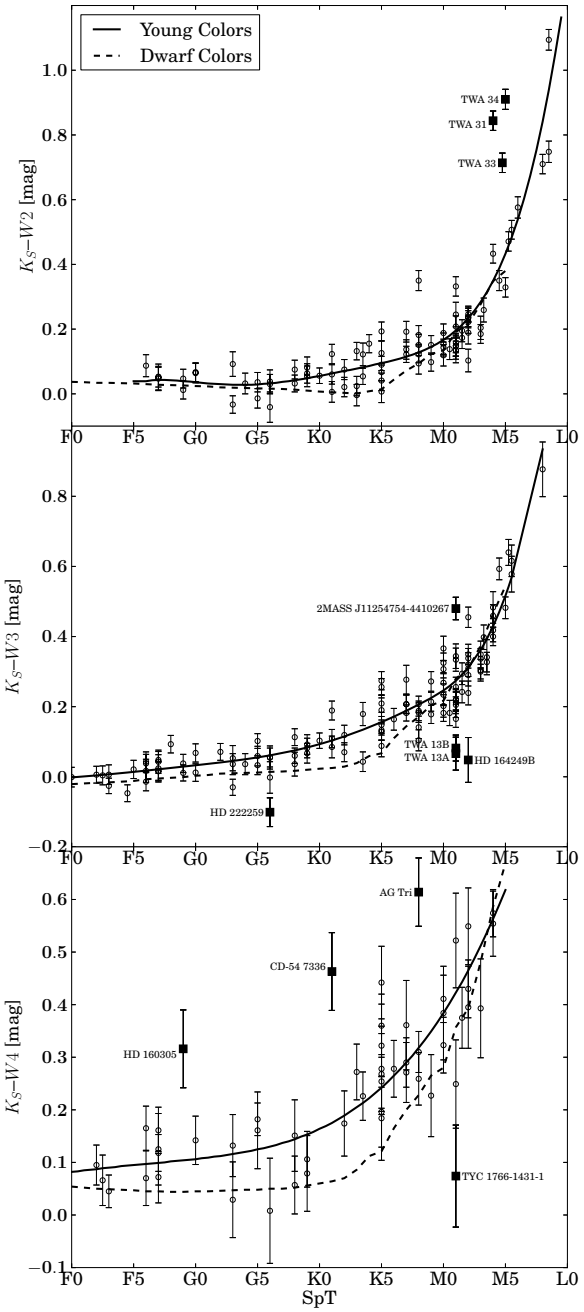

Figure 5. Same as in Figure 4, except showing colors $K_S - W2$, $K_S - W3$, and $K_S - W4$. Outliers (filled squares) have been excluded from the fit, and objects with known infrared excesses are not shown.

4.5.3. Analysis

For many objects in our sample, one or more bands of photometry are not available. In those cases we simply omit the term containing the missing band data. We do not fit bands with poor quality photometry (in 2MASS, anything other than quality flag "A"; for *WISE* bands, anything other than contamination and confusion flag "0"). We have again excluded photometry for objects with infrared excesses, flagged in Table 1. RECX 11 and RECX 15 have K_S-band excesses, so we exclude them from SED fitting entirely. We also exclude TWA 30A due to its time variable extinction (Looper et al. 2010b) and TWA 30B due to the time variable near-infrared excess (Looper et al. 2010a). TWA 31, TWA 33, and TWA 34 have $W1$- and $W2$-band excesses (Figures 4 and 5) so we exclude their *WISE* $W1$, $W2$, $W3$, and $W4$ band photometry. This leaves TWA 31 and TWA 34 with only JHK_S photometry, so we exclude them entirely. TWA 29 had only 2MASS JHK_S photometry, and HD 139084B and HD 164249B had 2MASS photometry and only two bands of *WISE* photometry with large uncertainties (>0.1 mag), which resulted in poorly constrained temperatures (e.g., $\sigma_{T_{\rm eff}} > 300$ K) so we excluded them from SED fitting as well. Objects excluded from SED fitting are listed in Table 8. The behavior of χ^2 as a function of $T_{\rm eff}$ is consistent with Gaussian errors and χ^2 has a quadratic dependence on $T_{\rm eff}$ near the best-fit value. A representative SED from our sample with the observed and best-fit model are shown in Figure 6.

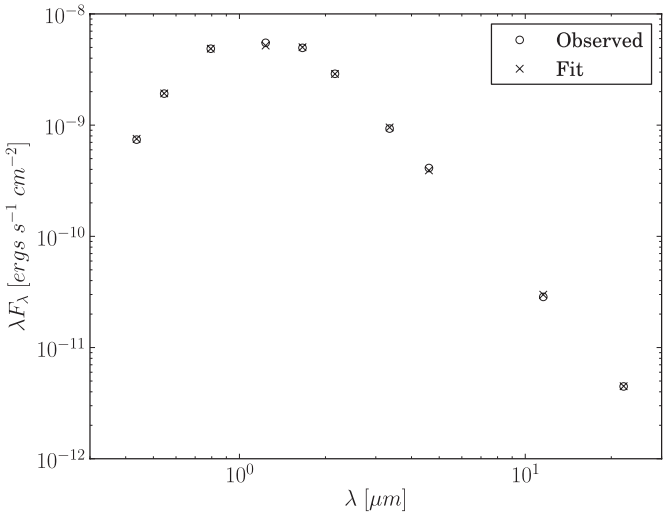

Figure 6. SED for β Pic member V1005 Ori (K8IVe). Observed photometry (circles) with the best fit BT-Settl model photometry (crosses) from a $T_{\rm eff} = 3866 \pm 18$ K model (interpolated). Uncertainties are smaller than the symbol markers.

In general the synthetic photometry is a function of $\log(g)$, $T_{\rm eff}$, and metallicity ([M/H]). As discussed previously, we use solar metallicity synthetic models. Pre-main-sequence evolutionary tracks from Baraffe et al. (1998) between 8–30 Myr predict that $\log(g)$ varies between 4.1 dex and 4.5 dex so we simply adopt 4.3 ± 0.2 dex. Though it is possible to fit both $T_{\rm eff}$ and $\log(g)$ simultaneously, this often gives spuriously large or small $\log(g)$ values, and even when the values of $\log(g)$ obtained from the fit are within an expected range, they are not well-constrained (e.g., formal errors on $\log(g) \sim 1.0$ dex). This is because most of the synthetic colors do not depend sensitively on the adopted $\log(g)$, and furthermore, we found that the best-fit $T_{\rm eff}$ did not vary significantly between $\log(g) = 4.1$ and $\log(g) = 4.5$. The mean difference in $T_{\rm eff}$ between $\log(g) = 4.1$ and 4.5 is 4 K with a dispersion of 31 K. Therefore, in our fitting procedure we set $T_{\rm eff}$ as the only free parameter. During the fitting procedure, we first determine $\mathcal{A}$ as the inverse-variance weighted mean difference between the observed and synthetic photometry at the stellar surface. However, rather than numerically minimizing χ^2 (as done in Masana et al. 2006) we simply find the minimum value over our grid, interpolated to $T_{\rm eff}$ increments of 20 K from 1400 K to 9800 K for the BT-Settl models and from 3500 K to 9750 K for the ATLAS9 models. We then fit a parabola in the region surrounding the minimum.

4.5.4. Results

The effective temperatures from the SEDF technique are listed in Table 9. We estimate our uncertainties by performing

Table 6
Intrinsic Colors of 5–30 Myr Old Stars and Adopted $T_{\rm eff}$, Bolometric Correction Values

Spec. Type	$T_{\rm eff}$ (K)	$B-V$ (mag)	$V-I_C$ (mag)	$V-K_S$ (mag)	$J-H$ (mag)	$H-K_S$ (mag)	K_S-W1 (mag)	K_S-W2 (mag)	K_S-W3 (mag)	K_S-W4 (mag)	BC_V (mag)	BC_J (mag)
F0	7280	0.28	0.34	0.73	0.11	0.06	0.04	0.03	0.00	0.08	0.01	0.57
F1	6990	0.34	0.39	0.89	0.14	0.07	0.04	0.04	0.00	0.09	0.00	0.68
F2	6710	0.38	0.43	0.99	0.15	0.08	0.04	0.05	0.00	0.09	−0.01	0.75
F3	6660	0.41	0.45	1.01	0.16	0.08	0.04	0.05	0.01	0.09	−0.01	0.76
F4	6590	0.43	0.48	1.05	0.17	0.08	0.04	0.06	0.01	0.09	−0.01	0.79
F5	6420	0.47	0.51	1.14	0.19	0.08	0.04	0.03	0.01	0.10	−0.02	0.85
F6	6250	0.50	0.55	1.25	0.21	0.09	0.04	0.04	0.02	0.10	−0.04	0.91
F7	6140	0.53	0.58	1.31	0.22	0.09	0.05	0.04	0.02	0.10	−0.05	0.95
F8	6100	0.55	0.60	1.34	0.23	0.09	0.05	0.04	0.03	0.10	−0.06	0.96
F9	6090	0.56	0.62	1.35	0.23	0.09	0.05	0.04	0.03	0.10	−0.06	0.97
G0	6050	0.57	0.66	1.37	0.24	0.09	0.06	0.04	0.03	0.11	−0.06	0.98
G1	5970	0.59	0.67	1.42	0.25	0.10	0.06	0.03	0.04	0.11	−0.07	1.00
G2	5870	0.60	0.71	1.49	0.27	0.10	0.07	0.03	0.04	0.11	−0.09	1.03
G3	5740	0.63	0.72	1.58	0.29	0.10	0.07	0.03	0.05	0.12	−0.11	1.08
G4	5620	0.66	0.73	1.68	0.31	0.11	0.07	0.03	0.05	0.12	−0.14	1.12
G5	5500	0.70	0.76	1.77	0.33	0.11	0.08	0.03	0.06	0.13	−0.17	1.16
G6	5390	0.74	0.79	1.86	0.35	0.12	0.08	0.03	0.06	0.13	−0.20	1.19
G7	5290	0.77	0.83	1.95	0.37	0.12	0.09	0.04	0.07	0.14	−0.23	1.23
G8	5210	0.79	0.87	2.02	0.39	0.12	0.09	0.04	0.08	0.14	−0.26	1.25
G9	5120	0.80	0.91	2.10	0.41	0.13	0.09	0.05	0.08	0.15	−0.29	1.27
K0	5030	0.82	0.93	2.19	0.43	0.13	0.09	0.06	0.09	0.16	−0.33	1.30
K1	4920	0.86	0.96	2.32	0.46	0.14	0.09	0.06	0.10	0.18	−0.38	1.34
K2	4760	0.93	1.01	2.49	0.49	0.14	0.09	0.07	0.12	0.19	−0.46	1.40
K3	4550	1.02	1.12	2.75	0.55	0.16	0.09	0.08	0.13	0.21	−0.60	1.44
K4	4330	1.11	1.27	3.06	0.60	0.17	0.09	0.09	0.14	0.22	−0.77	1.52
K5	4140	1.18	1.44	3.35	0.64	0.18	0.09	0.10	0.16	0.24	−0.95	1.58
K6	4020	1.24	1.57	3.54	0.66	0.19	0.10	0.10	0.17	0.27	−1.08	1.61
K7	3970	1.28	1.66	3.62	0.66	0.19	0.10	0.12	0.19	0.29	−1.14	1.63
K8	3940	1.32	1.74	3.67	0.67	0.20	0.10	0.13	0.21	0.32	−1.17	1.63
K9	3880	1.37	1.83	3.77	0.67	0.20	0.11	0.15	0.23	0.35	−1.24	1.66
M0	3770	1.41	1.95	3.96	0.68	0.21	0.11	0.17	0.25	0.38	−1.38	1.69
M1	3630	1.45	2.11	4.22	0.68	0.22	0.12	0.20	0.27	0.42	−1.58	1.74
M2	3490	1.46	2.28	4.50	0.67	0.23	0.14	0.23	0.31	0.47	−1.80	1.80
M3	3360	1.47	2.48	4.78	0.66	0.25	0.16	0.28	0.36	0.51	−2.03	1.84
M4	3160	1.53	2.78	5.23	0.62	0.27	0.19	0.35	0.43	0.56	−2.43	1.91
M5	2880	1.65	3.31	6.08	0.55	0.31	0.22	0.43	0.52	0.62	−3.21	2.01
M6	...	...	...	7.38	0.54	0.36	0.27	0.54	0.63	...	...	...
M7	...	...	...	8.47	0.58	0.41	0.33	0.67	0.77	...	...	...
M8	...	...	...	9.28	0.65	0.45	0.40	0.84	0.93	...	...	...
M9	...	...	...	9.80	0.70	0.47	0.49	1.05	1.13	...	...	...

(This table is also available in a machine-readable form in the online journal.)

a Monte Carlo simulation. For each object, we select trial photometry values from a distribution with mean and standard deviation equal to the observed photometry value and uncertainty, and use the trial photometry values to obtain the best-fit $T_{\rm eff}$ and angular diameter estimate. We perform 300 trials for each object and use the standard deviation of the resulting $T_{\rm eff}$ and angular diameter distribution as our statistical uncertainties. However, this does not account for systematics caused by uncertainties in our assumed surface gravity and metallicity. To account for these systematics, we repeat our fitting procedure for each object, varying $\log(g)$ from 4.1 dex to 4.5 dex and [m/H] from +0.2 dex to −0.2 dex. We adopt the dispersion in $T_{\rm eff}$ and angular diameter obtained for the systematic uncertainty, *typically* ∼ 11 K in $T_{\rm eff}$ and ∼1 μas in angular diameter. The uncertainties quoted in Table 9 are the statistical and (internal) systematic uncertainties added in quadrature. This does not account for any systematic uncertainties from the underlying Phoenix/NextGen models or the assumed solar abundances.

Similar to other studies, we find that $V-K_S$ provides the closest correlation to temperature with relatively little scatter. To take advantage of the utility of $V-K_S$ as a proxy for $T_{\rm eff}$, we estimate the spectral type–temperature calibration by fitting a polynomial to $T_{\rm eff}$ as a function of $V-K_S$. The coefficients for this polynomial are listed in Table 10. We then apply this polynomial to our spectral type–intrinsic color sequence. Unfortunately, only one object in our sample later than spectral type M5.5 has V-band photometry, so we do not provide effective temperature estimates for spectral types M6–M9, though we do provide intrinsic colors for those spectral types. Our spectral type, intrinsic color and $T_{\rm eff}$ sequence for young stars is listed in Table 6. For comparison, in Figure 7 we have plotted the new temperature scale for 5–30 Myr pre-MS stars described in this work, the giant temperature scale of van Belle et al. (1999), a new "consensus" dwarf $T_{\rm eff}$ scale described in Appendix C, and the young star scale of Luhman et al. (2003) (appropriate for ∼1 Myr old stars) as a function of spectral type. Our pre-MS

Table 7
$T_{\rm eff}$ Comparison: SEDF versus Diameter-derived $T_{\rm eff}$

Object	SpT	Ref.	$T_{\rm eff}$[a] (K)	$T_{\rm eff}$[b] (K)	$m_{\rm bol}$[c] (mag)
GJ 15A	M1.5V	1	3535 ± 14	3567 ± 11	6.560 ± 0.014
GJ 33	K2.5V	2	5047 ± 19	4950 ± 14	5.459 ± 0.017
GJ 53A	K1V Fe-2	3	5362 ± 22	5348 ± 26	4.981 ± 0.016
GJ 75	G9V	3	5395 ± 20	5398 ± 75	5.452 ± 0.018
GJ 105	K3V	2	4827 ± 18	4662 ± 17	5.406 ± 0.015
GJ 144	K2V(k)	2	5097 ± 19	5077 ± 35	3.457 ± 0.016
GJ 166A	K0.5V	2	5162 ± 21	5147 ± 14	4.169 ± 0.016
GJ 205	M1.5V	1	3703 ± 36	3801 ± 9	6.443 ± 0.016
GJ 338A	M0.0V	1	3896 ± 24	3907 ± 35	6.471 ± 0.017
GJ 338B	K7.0V	1	3887 ± 25	3867 ± 37	6.479 ± 0.017
GJ 380	K8V	3	4039 ± 23	4085 ± 14	5.544 ± 0.016
GJ 411	M2.0V	1	3481 ± 14	3464 ± 15	5.873 ± 0.015
GJ 412A	M1.0V	1	3584 ± 13	3497 ± 39	7.308 ± 0.014
GJ 436	M3.0V	1	3419 ± 17	3416 ± 53	8.778 ± 0.011
GJ 526	M1.5V	1	3642 ± 15	3618 ± 31	7.028 ± 0.013
GJ 551	M5.5V	1	2739 ± 12	3054 ± 79	7.280 ± 0.010
GJ 570A	K4V	2	4627 ± 16	4507 ± 58	5.245 ± 0.013
GJ 581	M2.5V	1	3304 ± 13	3442 ± 54	8.560 ± 0.010
GJ 631	K0V(k)	2	5272 ± 19	5337 ± 41	5.527 ± 0.017
GJ 687	M3.0V	1	3377 ± 13	3413 ± 28	7.231 ± 0.010
GJ 699	M4.0V	1	3089 ± 11	3222 ± 10	7.173 ± 0.012
GJ 725A	M3.0V	1	3316 ± 12	3407 ± 15	7.007 ± 0.014
GJ 725B	M3.5V	1	3218 ± 12	3104 ± 28	7.587 ± 0.013
GJ 764	K0V	4	5364 ± 21	5246 ± 26	4.498 ± 0.018
GJ 809	M0.0V	1	3715 ± 14	3692 ± 22	7.205 ± 0.011
GJ 820A	K5V	3	4498 ± 14	4361 ± 17	4.599 ± 0.014
GJ 820B	K7V	3	4117 ± 23	3932 ± 25	5.082 ± 0.019
GJ 845	K4V(k)	2	4713 ± 16	4555 ± 24	4.217 ± 0.014
GJ 880	M1.5V	1	3656 ± 16	3713 ± 11	4.217 ± 0.014
GJ 887	M2V	5	3617 ± 19	3676 ± 35	5.871 ± 0.015
GJ 892	K3V	3	4878 ± 18	4699 ± 16	5.191 ± 0.016

Notes.
[a] $T_{\rm eff}$ from this work using the SEDF method. See Section 4.5.2 for details.
[b] $T_{\rm eff}$ from Boyajian et al. (2012b) computed using direct angular diameter measurements.
[c] Apparent bolometric magnitude estimated from our SED fit.
Spectral Type References: (1) Henry et al. 2002; (2) Gray et al. 2006; (3) Gray et al. 2003; Keenan & McNeil 1989; (5) Torres et al. 2006.

Table 8
Objects Rejected from SED-$T_{\rm eff}$ Fitting

Object	Rejection Reason
HD 139084B	Uncertain photometry resulting in poorly constrained $T_{\rm eff}$
HD 164249B	Uncertain photometry resulting in poorly constrained $T_{\rm eff}$
RECX 11	K_S band excess
RECX 15	K_S band excess
RECX 16	*IRAC* 3.6 μm and 4.5 μm excess
TWA 27	*IRAC* 3.6 μm and 4.5 μm excess
TWA 29	Only three good bands of photometry (JHK_S)
TWA 30A	Time-variable extinction
TWA 30B	Time-variable NIR excess
TWA 31	Only three good bands of photometry (JHK_S)
TWA 34	Only three good bands of photometry (JHK_S)

$T_{\rm eff}$ scale is within ∼100 K of the dwarf scale as a function of spectral type, except for spectral types G5 through K6, which are ∼250 K cooler than their MS counterparts.

4.6. Bolometric Corrections

As a byproduct of estimating the effective temperature of stars in our sample using the method of SED fitting, we also obtain an estimate of each object's angular diameter. This can then be used to estimate the apparent bolometric magnitude ($m_{\rm bol}$) and the bolometric correction in any band (BC$_x$). The basic equation that relates stellar bolometric magnitude to luminosity is

$$M_{\rm bol} = -2.5\log\left(\frac{L}{L_\odot}\right) + M_{\rm bol,\odot}$$
$$= -10\log\left(\frac{T_{\rm eff}}{T_\odot}\right) - 5\log\left(\frac{R}{R_\odot}\right) + M_{\rm bol,\odot}.$$

We can also write this in terms of apparent magnitude m_x in band x with the distance d and bolometric correction BC$_x$:

$$M_{\rm bol} = m_x - 5\log\left(\frac{d}{10\,{\rm pc}}\right) + {\rm BC}_x.$$

Equating these two, using the angular semi-diameter $\theta = (R/d) = 10^{-0.2\mathcal{A}}$, and solving for BC$_x$ we find

$${\rm BC}_x = \mathcal{A} + 5\log\left(\frac{R_\odot}{10\,{\rm pc}}\right) + M_{\rm bol,\odot}$$
$$- 10\log\left(\frac{T_{\rm eff}}{T_{\rm eff,\odot}}\right) - m_x.$$

We use consistent solar values of $T_{\rm eff,\odot} = 5772$ K, $R_\odot = 695660$ km, $m_{V,\odot}$ from Section 4.5.2, and $M_{\rm bol,\odot} = 4.755$ mag as adopted by Mamajek (2012).[11] The uncertainties in BC$_x$ are

$$(\sigma_{{\rm BC}_x})^2 = \left(\frac{10\sigma_{T_{\rm eff}}}{T_{\rm eff}\ln 10}\right)^2 + (\sigma_{\mathcal{A}})^2 + (\sigma_{m_x})^2.$$

Though the zero point of the BC scale is arbitrary, the combination of BC and solar absolute bolometric magnitude is not (see Torres 2010 and Appendix D of Bessell et al. 1998). In Table 9 we give the calculated individual BCs in both

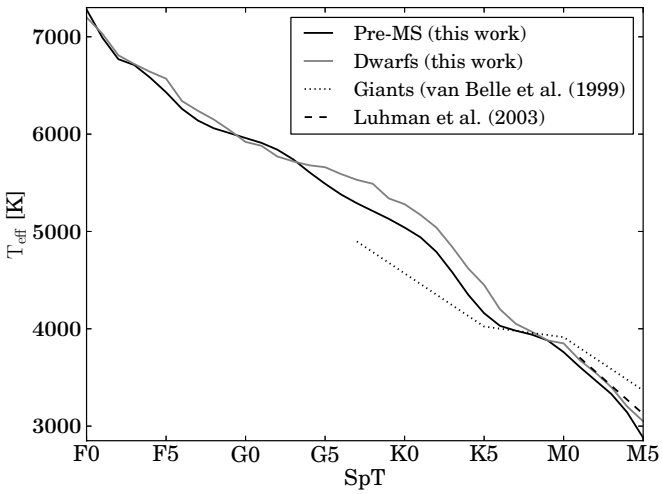

Figure 7. Spectral type vs. $T_{\rm eff}$ for the pre-MS (solid black line) and dwarf (solid gray line) $T_{\rm eff}$ scales derived in this work. For comparison we plot the giant $T_{\rm eff}$ scale of van Belle et al. (1999) (dotted line) and the $T_{\rm eff}$ scale of Luhman et al. (2003) (dashed line), appropriate for ∼1 Myr old stars. Our pre-MS $T_{\rm eff}$ scale is within 100 K of the dwarf scale as a function of spectral type, except for spectral types G5 through K6, which are ∼250 K cooler than their MS counterparts.

[11] See also "Basic Astronomical Data for the Sun," https://sites.google.com/site/mamajeksstarnotes/basic-astronomical-data-for-the-sun more complete discussion on solar data, including motivation for the values adopted here.

Table 9
$T_{\rm eff}$, Bolometric Magnitudes, Bolometric Corrections, and Angular Diameter Estimates from SED Fitting

Object	2MASS	BT-Settl						Kurucz					
		$T_{\rm eff}$ (K)	θ (μas)	BC$_V$ (mag)	BC$_J$ (mag)	$m_{\rm bol}$ (mag)	$\log(L/L_\odot)$ (dex)	$T_{\rm eff}$ (K)	θ (μas)	BC$_V$ (mag)	BC$_J$ (mag)	$m_{\rm bol}$ (mag)	$\log(L/L_\odot)$ (dex)
HIP 490	00055255-4145109	5990 ± 16	250 ± 1	-0.06 ± 0.02	0.98 ± 0.02	7.45 ± 0.02	0.114 ± 0.048	5968 ± 15	250 ± 1	-0.05 ± 0.02	1.00 ± 0.02	7.46 ± 0.02	0.108 ± 0.047
HR 9	00065008-2306271	6796 ± 25	346 ± 1	0.00 ± 0.02	0.74 ± 0.03	6.19 ± 0.02	0.617 ± 0.033	6773 ± 21	348 ± 1	0.01 ± 0.02	0.75 ± 0.03	6.20 ± 0.02	0.614 ± 0.032
HIP 1113	00135300-7441178	5434 ± 15	180 ± 1	-0.17 ± 0.02	1.18 ± 0.03	8.59 ± 0.02	-0.238 ± 0.074	5401 ± 16	180 ± 1	-0.15 ± 0.02	1.21 ± 0.03	8.61 ± 0.02	-0.247 ± 0.074
HIP 1481	00182612-6328389	6150 ± 18	242 ± 1	-0.06 ± 0.02	0.94 ± 0.02	7.41 ± 0.02	0.177 ± 0.045	6123 ± 17	242 ± 1	-0.04 ± 0.02	0.96 ± 0.02	7.42 ± 0.02	0.171 ± 0.045
TYC 1186-706-1	00233468+2014282	4055 ± 15	189 ± 1	-1.09 ± 0.10	1.61 ± 0.03	9.75 ± 0.03	...	3888 ± 42	197 ± 1	-1.00 ± 0.11	1.70 ± 0.05	9.84 ± 0.05	...
HIP 1910	00240899-6211042	3823 ± 18	188 ± 2	-1.31 ± 0.02	1.64 ± 0.03	10.02 ± 0.03	-0.659 ± 0.288	3805 ± 24	189 ± 2	-1.31 ± 0.02	1.64 ± 0.03	10.03 ± 0.02	-0.660 ± 0.288
HIP 1993	00251465-6130483	4015 ± 14	159 ± 1	-1.09 ± 0.03	1.56 ± 0.03	10.17 ± 0.03	-0.845 ± 0.222	3975 ± 17	161 ± 1	-1.07 ± 0.03	1.57 ± 0.03	10.19 ± 0.03	-0.850 ± 0.222
HIP 2729	00345120-6154583	4376 ± 10	252 ± 1	-0.76 ± 0.02	1.46 ± 0.02	8.80 ± 0.02	-0.330 ± 0.087	4318 ± 9	256 ± 1	-0.74 ± 0.01	1.48 ± 0.02	8.82 ± 0.02	-0.339 ± 0.087
HIP 3556	00452814-5137339	3576 ± 23	190 ± 2	-1.63 ± 0.02	1.80 ± 0.02	10.28 ± 0.03	-0.998 ± 0.214	3590 ± 32	190 ± 3	-1.64 ± 0.02	1.79 ± 0.02	10.27 ± 0.02	-0.993 ± 0.214
TYC 5853-1318-1	01071194-1935359	3782 ± 33	208 ± 1	-1.61 ± 0.08	1.70 ± 0.04	9.85 ± 0.05	...	3686 ± 29	214 ± 2	-1.56 ± 0.08	1.74 ± 0.04	9.89 ± 0.04	...

Notes. $T_{\rm eff}$ values were fit at $\log(g) = 4.3$. In addition, we have used a weighted mean distance of 94.3 ± 1.2 pc for η Cha cluster members. For HD 139084B, HD 164249B, AZ Cap, and HD 222259B we have adopted parallaxes from their brighter companions.

[a] Indicates $\log(L/L_\odot)$ estimates use parallaxes from Weinberger et al. (2013).

[b] Indicates $\log(L/L_\odot)$ estimate uses parallax from Teixeira et al. (2008).

[c] Indicates $\log(L/L_\odot)$ estimate uses parallax from Teixeira et al. (2009).

(This table is available in its entirety in a machine-readable form in the online journal. A portion is shown here for guidance regarding its form and content.)

Table 10
$T_{\rm eff}$, Bolometric Correction, and Bolometric Magnitude Polynomial Coefficients for 5–30 Myr Old Stars

Y	X	Range	a_0	a_1	a_2	a_3	a_4	a_5	a_6	a_7
$T_{\rm eff}$	$V-K_S$	$1.0 < V-K_S < 6.7$	9.323430×10^3	-3.516011×10^3	1.046787×10^3	-1.863349×10^2	1.641182×10^1	-5.188853×10^{-1}	...	...
$T_{\rm eff}$	$V-J$	$0.8 < V-J < 5.8$	9.593475×10^3	-5.095204×10^3	2.053259×10^3	-4.813940×10^2	5.816754×10^1	-2.779565×10^0	...	...
BC$_V$	$V-K_S$	$1.0 < V-K_S < 6.7$	-7.443324×10^{-2}	2.471780×10^{-1}	-1.923234×10^{-1}	1.318867×10^{-2}	-3.630511×10^{-4}	...	...	...
BC$_V$	$T_{\rm eff}$	$2750 < T_{\rm eff} < 7350$	-2.855844×10^2	3.832453×10^{-1}	-2.225832×10^{-4}	7.150667×10^{-8}	$-1.364193 \times 10^{-11}$	1.542389×10^{-15}	$-9.566224 \times 10^{-20}$	2.511807×10^{-24}
BC$_J$	$V-K_S$	$1.0 < V-K_S < 6.7$	-4.805196×10^{-1}	1.842350×10^0	-7.837156×10^{-1}	1.859281×10^{-1}	-2.153500×10^{-2}	9.489583×10^{-4}	...	...
BC$_J$	$V-J$	$0.8 < V-J < 5.8$	-4.557821×10^{-1}	2.299875×10^0	-1.191653×10^0	3.442879×10^{-1}	-4.932544×10^{-2}	2.724400×10^{-3}	...	...
BC$_J$	$T_{\rm eff}$	$2750 < T_{\rm eff} < 6750$	2.920272×10^0	-3.220428×10^{-4}	...	...	...	...	...	...

Note. $Y = a_0 + a_1 X + a_2 X^2 + a_3 X^3 + a_4 X^4 + a_4 X^4 + a_5 X^5 + a_6 X^6 + a_7 X^7$.

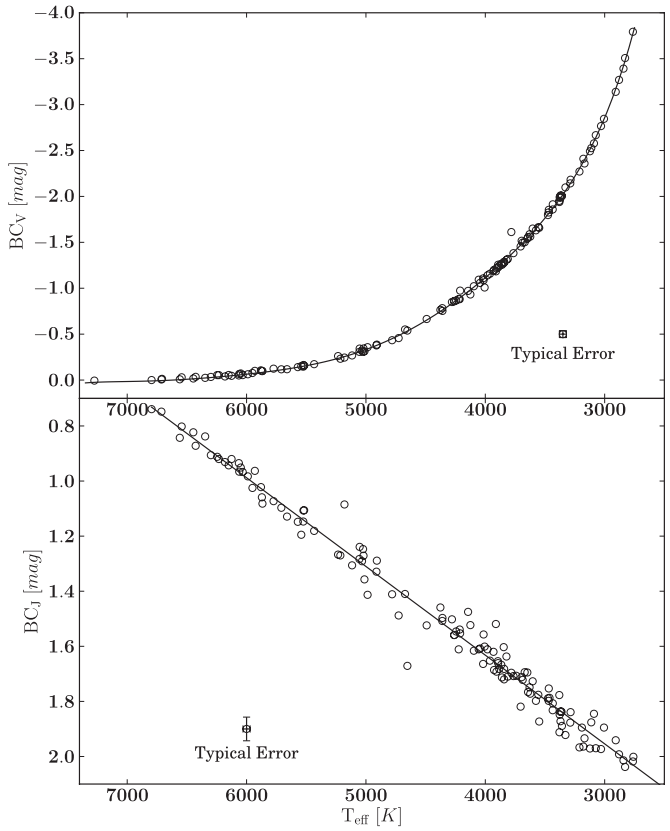

Figure 8. Bolometric corrections for V and J band magnitudes as a function of effective temperature. Note that for $T_{\rm eff} \lesssim 5000$ K, BC$_V$ becomes a sensitive function of $T_{\rm eff}$ and therefore it is preferable to use $M_{\rm bol} = M_J + {\rm BC}_J$ for cooler stars. Coefficients for polynomial fit are listed in Table 10.

Johnson V band and 2MASS J band. We also provide $\log(L/L_\odot)$ for stars with measured trigonometric parallaxes. For F- and G-type stars ($T_{\rm eff} \gtrsim 5000$ K) it is preferred to estimate bolometric magnitudes using $M_{\rm bol} = M_V + {\rm BC}_V$ since the V band correction is not a sensitive function of $T_{\rm eff}$ for 5000 K $< T_{\rm eff} <$ 7000 K. However, for K- and M-type stars ($T_{\rm eff} \lesssim 5000$ K) BC$_V$ becomes a steep function of $T_{\rm eff}$ and therefore it is better to use $M_{\rm bol} = M_J + {\rm BC}_J$. Plots of BC$_V$ and BC$_J$ versus $T_{\rm eff}$ are shown in Figure 8. Polynomial fits to BC$_V$ and BC$_J$ as a function of $T_{\rm eff}$ and $V - K_S$ are given in Table 10.

5. DISCUSSION

Consistent with previous studies (e.g., Da Rio et al. 2010; Luhman et al. 2010b), we have found that pre-MS stars do not have the same intrinsic colors as field dwarfs for certain spectral types and colors. There are two likely main reasons for the differences in colors. The first and most important cause is the different surface gravities of pre-MS stars compared to MS dwarfs. The striking bifurcation in the $V - K_S$ versus $J - H$ color–color diagram between dwarfs and giants has been explained as an effect of CO and H_2O bands and H^- opacity (Jorgensen 1996). The $B - V$ colors for pre-MS stars with $V - K_S > 3.0$ are systematically bluer than MS stars. At lower surface gravities, the synthetic BT-Settl $B - V$ colors are predicted to be bluer at a given $V - K_S$ than higher-surface gravity stars. Our new spectral type–color relations take these important surface-gravity effects for young stars into account. However, this does not explain the origin of redder colors, particularly $H - K_S$, for F- and G-type stars, which have surface gravities very close to MS dwarfs.

The second possible explanation for color differences between young stars and older MS stars suggested by Gullbring et al. (1998) and Stauffer et al. (2003) is the greater abundance of stellar spots on young stars. Young stars show evidence of stronger magnetic activity than older MS stars, which is exhibited by hotter plage and cooler spot regions on the surface. In particular, these plage regions have been suggested as contributing to the systematically bluer $B - V$ colors observed in the Pleiades open cluster (Stauffer et al. 2003). Gullbring et al. (1998) estimated a ~50% spot coverage to account for the mean $V - J$ color anomaly in weak-lined T Tauri stars. However, the Stauffer et al. (2003) study is the most comprehensive attempt to date to investigate the contribution of cool spots to stellar colors. Stauffer et al. (2003) found that Pleiades K star red spectra (5700–8400 Å) had systematically later spectral types than the blue (3300–5300 Å) spectra, whereas the older Praesepe K stars did not suffer from this effect.[12] Stauffer et al. (2003) additionally modeled the *BVRIJHK* SEDs of several Pleiades, combining observed SEDs of an earlier field dwarf and a later field dwarf to obtain a fit. The best-fit models obtained in the Stauffer et al. (2003) study indicated that the K-type Pleiades were covered in $\gtrsim$50% "cool spots," consistent with the Gullbring et al. (1998) results. They use *BVRIJHK* photometry to fit observed Pleiad SEDs. On the basis of their spectroscopy and SED fitting, Stauffer et al. (2003) concluded that the Pleiades K stars had more than one photospheric temperature, and that spottedness was well-correlated with the $B - V$ color anomaly. While these results point convincingly to stellar spots as a significant contributing factor, especially to bluer $B - V$ colors, we do not attempt to quantify the relative contribution of spots or surface gravity effects to the intrinsic colors of pre-MS stars. Disentangling the effects of surface gravity and spots would require time-series multi-band photometry for most of the objects in our sample. Quantifying the specific contribution of the spots and plages to the stellar colors is beyond the scope of this study.

McCarthy & White (2012) published predicted angular diameters for many of the β Pic moving group members in our sample using estimated H-R diagram positions and revised *Hipparcos* parallaxes (van Leeuwen 2007). In addition, Lafrasse et al. (2010) have estimated the angular diameters of thousands of dwarfs and giants with V and $V - K$ surface brightness relations (e.g., Barnes & Evans 1976). We compare our results to the McCarthy & White (2012) and Lafrasse et al. (2010) results in Figure 9. Our angular diameter estimates follow the Lafrasse et al. (2010) estimates very closely, though ours are systematically smaller by 4%. There is a trend with $T_{\rm eff}$, with hotter objects tend to be more discrepant than cooler objects, however, the origin of this discrepancy is unclear. Our angular diameter estimates also compare well with the results of McCarthy & White (2012), with our estimates being 6% larger on average, but with much larger scatter, however, this difference is not statistically significant. The larger scatter between our angular diameter estimates and those from McCarthy & White (2012) are likely due to the different methods used to infer the stellar $T_{\rm eff}$s. For example, we predict TYC 1208-468-1 to have a diameter of 241 ± 1 μas, but McCarthy & White (2012) predict 120 μas. This star has *BVJHK* colors consistent with a spectral

[12] This effect is also seen in G and K stars from the younger Scorpius-Centaurus OB association, where blue spectra (~3800–5400 Å) give systematically earlier spectral types than the red spectra (~6200–7100 Å) by about one spectral subtype (E. E. Mamajek 2012, private communication).

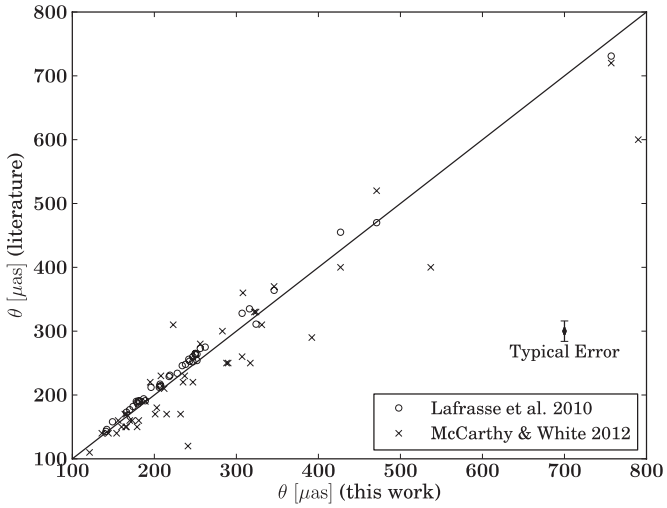

Figure 9. The individual angular diameter estimates from this work compared with estimates from McCarthy & White (2012) and Lafrasse et al. (2010).

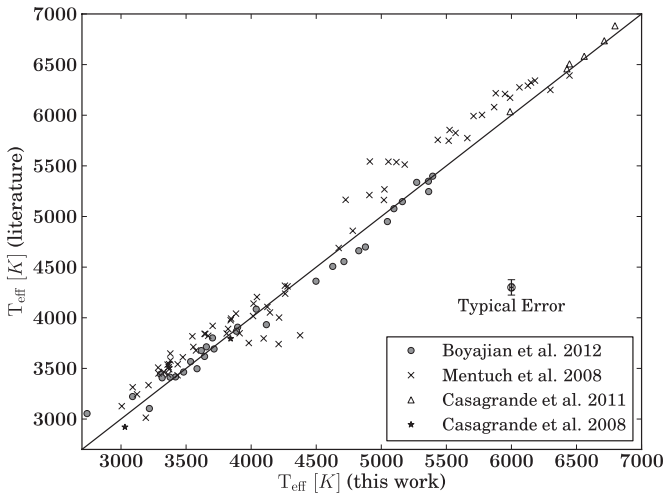

Figure 10. The individual $T_{\rm eff}$ values from this work compared with values obtained by least-squares fitting to synthetic NextGen spectra from Mentuch et al. (2008; crosses) and those in the study of Casagrande et al. (2011; triangles) and Casagrande et al. (2008; stars). We also compare a sample of K- and M-type dwarfs which have angular diameter-based $T_{\rm eff}$ estimates from Boyajian et al. (2012b) with estimates using our SEDF implementation (circles). The values in Mentuch et al. (2008) are systematically higher than those estimated in this work, with the difference ∼230 K above 4500 K, reducing to ∼120 K below 4500 K. Those from the Casagrande et al. (2011) study are typically ∼40 K higher than the values from this work.

type of ∼K6, but it has a reported spectral type of K3Ve (Jeffries 1995). The ∼600 K difference in the assumed $T_{\rm eff}$ translates to a large difference in the predicted angular diameter.

There is considerable overlap between our sample and the sample of Mentuch et al. (2008), who examined Li depletion in several nearby young associations. The Mentuch et al. (2008) study estimated $T_{\rm eff}$ for each star in their sample by least-squares fitting synthetic spectra to spectral regions λλ5850–5930, 7900–7980, 8150–8230, 8400–8480, and 8485–8565 generated with NextGen model atmospheres. In Figure 10 we compare our $T_{\rm eff}$ values obtained by fitting multi-band photometry to the BT-Settl NextGen model colors with the $T_{\rm eff}$ values obtained by Mentuch et al. (2008). Overall there is a systematic difference—the values obtained by Mentuch et al. (2008) are systematically ∼150 K hotter than the values we obtain, with a larger difference (∼230 K) above 4500 K and a smaller difference (∼120 K) below 4500 K. This discrepancy could be due to the different synthetic models used. The latest BT-Settl models use the revised solar abundances from Asplund et al. (2009) and include more complete molecular opacity lists, though these updated opacities would mostly affect the lower-mass stars and are unlikely to account for the differences above ∼5000 K.

In addition we have compared our estimated $T_{\rm eff}$ values with those of Casagrande et al. (2008) and Casagrande et al. (2011), where possible (Figure 10). Both studies used synthetic spectra with an implementation of the IRFM or a closely related method (Multiple Optical Infrared TEchnique or "MOITE") to estimate the stellar effective temperature for a large number of objects. The IRFM compares the ratio of the observed bolometric flux to the observed monochromatic flux density at the Earth ("$R_{\rm obs}$") to the ratio of theoretical bolometric flux to monochromatic flux density at the surface of the star ($R_{\rm theo}$; Blackwell & Shallis 1977). $R_{\rm theo}$ is a function of the $T_{\rm eff}$, and is compared to the $R_{\rm obs}$ ratio to obtain the $T_{\rm eff}$ of the star. For hotter stars the sensitivity to the model in the IR is very minimal and thus only these flux ratios in IR bands are used to determine the $T_{\rm eff}$. For cooler stars, Casagrande et al. (2008) have adapted this method to use optical and infrared bands (called "MOITE"). Casagrande et al. (2008) assumed $\log(g) = 5.0$ dex throughout with the "Cond" variant of NextGen models (we have used the "BT-Settl" variant here with revised solar abundances from Asplund et al. 2009), whereas the Casagrande et al. (2011) study used the Castelli & Kurucz (2004) models which used the Grevesse & Sauval (1998) solar abundances. Stellar $T_{\rm eff}$ estimates from this work are typically ∼40 K lower than the values from the Casagrande et al. (2011) study (six stars in common), and within 2σ of the values from the Casagrande et al. (2008) study (stars TX PsA and HIP 107345 in common). A comparison of stellar $T_{\rm eff}$ estimates from this work and the literature is shown in Figure 10.

For the few objects with spectral types M8 or later we obtain cooler temperatures than expected from the temperature scale of Luhman et al. (2003) or the dwarf temperature scale. Rice et al. (2010a) fit PHOENIX dusty synthetic spectra to high-resolution observed spectra to find the best-fit $T_{\rm eff}$ and $\log(g)$ of sample of young late M-type objects. Two objects in our sample with SEDF-determined $T_{\rm eff}$, 2MASS J06085283-2753583 (2M0608-27; M8.5γ; Rice et al. 2010b) and TWA 26 (M8IVe; Barrado Y Navascués 2006), are included in the Rice et al. (2010a) study. For 2M0608-27, assuming $\log(g) = 4.3$ dex, we find $T_{\rm eff} = 2118 \pm 20$ K, whereas Rice et al. (2010a) adopt $\log(g) = 3.98$ and $T_{\rm eff} = 2529$ K, much hotter than our results and consistent with the temperature scale of Luhman et al. (2003). We find $T_{\rm eff} = 2176 \pm 17$ K for TWA 26 but Rice et al. (2010a) find $\log(g) = 3.98$ and $T_{\rm eff} = 2609$ K, again much hotter than our results and consistent with the $T_{\rm eff}$ scale of Luhman et al. (2003). These four objects lack BVI_C photometry and thus do not have any SED fitting constraints blueward of their SED peak; this could be a contributing factor in their discrepantly cool $T_{\rm eff}$ fit. Because of these discrepancies, we do not include $T_{\rm eff}$ estimates for M6 through M9 objects in our pre-MS temperature scale (Table 6).

Only two stars in our sample, HR 9 and 51 Eri, have direct angular diameter measurements available from the literature. Simon & Schaefer (2011) measured angular diameters of 492 ± 32 μas and 518 ± 9 μas for HR 9 and 51 Eri, respectively. Our angular diameter estimates of 346 ± 1 μas for HR 9 and 471 ± 2 μas for 51 Eri are much lower than the interferometric measurements. While we have no reason to suspect the direct

measurements are unreliable a priori, the angular diameter of 492 μas for HR 9 (F3Vn; Gray et al. 2006) warrants some discussion. If we adopt the estimated bolometric flux at Earth for HR 9 from Casagrande et al. (2011) of 8.6609×10^{-8} mW m^{-2}, and again use the measured angular diameter of 492 μas, we obtain a $T_{\rm eff}$ of 5724 K, similar to a G3V! This is ~1000 K cooler than the 6883 ± 91 K estimated by Casagrande et al. (2011) and our estimate of 6761 ± 28 K, both of which are consistent with the F3Vn spectral type. The Simon & Schaefer (2011) results indicate a larger angular diameter at H band than K band, which points to unusual calibration errors (M. Simon 2012, private communication). We suspect that our predicted angular diameters are closer to the actual diameters and until updated measurements are published, we recommend our predicted angular diameter.

6. CONCLUSIONS

We can summarize our conclusions as follows:

1. 5–30 Myr old pre-MS stars follow slightly different spectral type–intrinsic color sequences than that of MS stars. Pre-MS colors follow the dwarf sequence for some colors and spectral types, but for other optical/infrared colors and spectral types, deviations can exceed 0.3 mag. In Table 6 we provide an empirical tabulation of the intrinsic colors of young stars for spectral types F0 through M9, including B-V, $V-I_C$, $V-K_S$, $J-H$, $H-K_S$, K_S-W1, K_S-W2, K_S-W3, and K_S-W4.
2. Consistent with previous findings (Luhman 1999; Da Rio et al. 2010), we find that color differences between K- and M-type pre-MS stars and dwarfs appear to be predominantly due to the young stars' lower surface gravities. This is demonstrated by theoretical models predicting redder $J-H$ colors and bluer $B-V$ colors for lower surface gravity objects, consistent with observations. However, we cannot exclude hotter plage and cooler spot regions on the stellar surface as contributing factors.
3. A pre-MS $T_{\rm eff}$ scale derived from fitting SEDs to synthetic spectral models is within ~100 K of MS stars as a function of $V-K_S$. As a function of spectral type, the effective temperatures of F0 through G4 and K7 through M5 pre-MS stars are within ~100 K of their MS counterparts, whereas G5 through K6 pre-MS stars are ~250 K cooler at a given spectral type. We provide new spectral type–$T_{\rm eff}$ relations and color–$T_{\rm eff}$ relations appropriate for 5–30 Myr old pre-MS stars. We also provide BCs appropriate for pre-MS stars as polynomial functions of $T_{\rm eff}$ and $V-K_S$ in Table 10 and as part of our spectral type–intrinsic color sequence in Table 6.

We thank Fred Walter for the use of his IDL reduction pipeline and the Stony Brook Spectral Standards Library. We also thank the referee, Kevin Luhman, for his very thorough and prompt review which greatly improved the paper. Spectra taken for this study were observed on the 1.5 m telescope on Cerro Tololo via the Small and Moderate Aperture Research Telescope System (SMARTS) Consortium. We thank Duy Nyugen for helpful discussions regarding χ^2 fitting. This work was supported by funds from NSF grant AST-1008908. This publication makes use of data products from the Two Micron All Sky Survey, which is a joint project of the University of Massachusetts and the Infrared Processing and Analysis Center/California Institute of Technology, funded by the National Aeronautics and Space Administration and the National Science Foundation. This publication makes use of data products from the *Wide-field Infrared Survey Explorer*, which is a joint project of the University of California, Los Angeles, and the Jet Propulsion Laboratory/California Institute of Technology, funded by the National Aeronautics and Space Administration. This research was made possible through the use of the AAVSO Photometric All-Sky Survey (APASS), funded by the Robert Martin Ayers Sciences Fund. This research used the Digitized Sky Survey, NASA ADS, and the SIMBAD and Vizier databases.

APPENDIX A

MEMBERSHIP OF TWA 9 TO THE TW Hya ASSOCIATION

The membership of TWA 9 to the TW Hya Association merits some discussion. Weinberger et al. (2013) showed that the space motion of TWA 9A is more than 3σ from the mean of the association, and concluded that it was either not a member or the *Hipparcos* distance is underestimated. However, when considering the TWA centroid space motion (Weinberger et al. 2013), the Tycho-2 proper motion ($\mu_{\alpha}* = -55.4 \pm 2.3$ mas yr^{-1}, $\mu_{\delta} = -17.7 \pm 2.3$ mas yr^{-1}; Høg et al. 2000) of TWA 9A seems consistent with membership in TWA. Assuming it is a member and adopting the TWA mean group space motions from Weinberger et al. (2013) of (U, V, W) = (−10.9 ± 0.2, −18.2 ± 0.2, −5.3 ± 0.2) km s^{-1}, we estimate a kinematic distance of 70.0 ± 3.8 pc, based on the method discussed in Mamajek (2005). If we adopt this kinematic distance with the Bailey et al. 2012 mean radial velocity for component A and B of 11.964 ± 0.024 km s^{-1}, the three-dimensional space motion of TWA 9A is then (U, V, W) = (−10.2 ± 1.2, −19.7 ± 0.8, −4.8 ± 0.6) km s^{-1}. This is consistent with the mean TWA space motions in the Weinberger et al. (2013) study. Furthermore, the kinematic distance would decrease the absolute magnitude M_H by ≈0.83 mag over the *Hipparcos* distance (using $d = \pi^{-1}$, where π is the trigonometric *Hipparcos* parallax), and thus the isochronal age of TWA 9A would be ~16 Myr, much closer to the isochronal ages obtained by Weinberger et al. (2013) for other TWA members. TWA 9A exhibits very high Li (EW(Li 6708 Å) = 470 m Å; Torres et al. 2006), lies in the direction of other TWA members, has proper motion consistent with membership in TWA, and, adopting the kinematic distance of 70.0 ± 3.8 pc, has a space motion and isochronal age consistent with membership in TWA. Thus, we retain TWA 9A and TWA 9B as members of TWA and suggest that the *Hipparcos* parallax is most likely ~3σ in error.

APPENDIX B

SPECTRAL TRANSITION FROM K7 TO M0

Some spectral surveys implicitly or explicitly do not recognize or use spectral types K8 and K9. While spectral types K8 and K9 are not considered full subtypes of the spectral classification system (Keenan 1984), it should be pointed out that neither are G1, G3, G4, G6, G7, or G9, yet these classifications are consistently recognized and used (e.g., Gray et al. 2003). Keenan (1984) noted that subdivisions such as G3 simply means the star is closer to G2 than G5, and that they should be used when it is possible to classify the stars accurately enough to justify their use. Keenan (1984) considered K5 and M0 one subtype apart even though the difference in their $B-V$ color is 0.3 mag, larger than the difference between M0 and M4 (see Table 5). From the standpoint of spectral classification, there is nothing

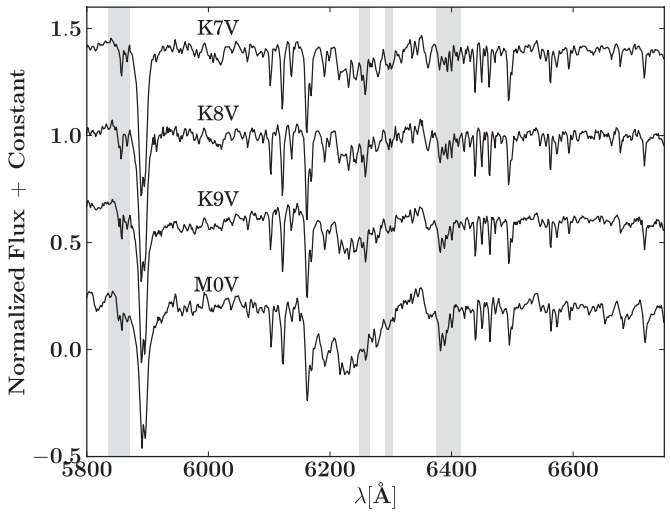

Figure 11. Spectral transition from K7 to M0, with regions most useful for discriminating among the different spectral types highlighted in gray. GJ 673 (K7V), HIP 111288 (K8Vk), HIP 3261 (K9V), and GJ 701 (M0.0V) are shown.

different about the K7 to M0 transition that merits such a gap in spectral types. Therefore we find no compelling reason to omit spectral types K8 and K9 from use and we include them here in our analysis.

With low-resolution red optical spectra we can distinguish between subtypes K7, K8, K9 and M0. Unfortunately, K8V and K9V spectral standards do not appear in the literature (e.g., Gray & Corbally 2009). For these subtypes, we adopted stars as standards which were assigned this classification by an expert classifier. For K8V we adopted HIP 111288 ($V - K_S = 3.52 \pm 0.02$ mag; Perryman & ESA 1997; Skrutskie et al. 2006), classified as K7V by Stephenson (1986) but later classified as K8Vk by Gray et al. (2006). For K9V we adopted HIP 3261 ($V - K_S = 3.70 \pm 0.02$ mag; Perryman & ESA 1997; Skrutskie et al. 2006), classified as K7.0 by Hawley et al. (1996) but later classified as K9V by Gray et al. (2006). These were chosen because they were classified as intermediate between K7 and M0 but also because they have $V - K_S$ colors intermediate between K7 and M0. We visually compared the spectra of both adopted standards and verified that they were morphologically intermediate between the K7V and M0V standards in Table 2.

Figure 11 shows the red spectral sequence from K7 to M0. The spectra show a distinct progression in the CaH band at λλ 6382–6389 (Kirkpatrick et al. 1991; Torres-Dodgen & Weaver 1993; Allen & Strom 1995) which gradually becomes stronger than the Fe I lines at 6400 Å and 6393 Å. Another very useful discriminant is the relative strength of the V, Ti, and Fe blend at 6297 Å to the Fe I blend at 6302 Å. As the TiO band ∼6080–6390 Å increases in strength going from the late K-types to M0, the relative strength of these two lines gradually changes, with the blend at 6297 Å becoming stronger at K8.

Lastly, we mention that skipping from K7 to M0 may hide important discrepancies between models and observations. Casagrande et al. (2008) has noted that, among MS dwarf stars, there appears to be a plateau in luminosity in the transition region between K and M where the stars appear to be decreasing in temperature with very little decrease in luminosity. Theoretical models do not appear to reproduce the plateau. Using subtypes K8 and K9, when possible, presents an opportunity for observational work to make contact with theoretical models in this region.

APPENDIX C

DWARF COLORS AND TEMPERATURES

In order to accurately compare the empirical intrinsic colors and $T_{\rm eff}$ scale of pre-MS stars to dwarfs and quantify their differences, the empirical intrinsic colors of dwarf stars must be accurately tabulated. Here we describe the construction of a modern dwarf color, $T_{\rm eff}$, and BC sequence, which has been an ongoing process carried out over several years. While other compilations are available (e.g., Schmidt-Kaler 1982; Kenyon & Hartmann 1995; Worthey & Lee 2011), it was our goal to incorporate a detailed review of the color/temperature placement of modern spectral standard stars and assess their pedigree as standards. A preliminary version of this sequence (A0V-G9V) was previously published in Pecaut et al. (2012). The primary motivations for constructing this sequence were that (1) color sequences over the O-M range of spectral types had not been constructed explicitly including 2MASS and *WISE* bands, (2) the methodology of the construction of previous sequences was not always made clear, (3) systematic differences exist between some of the widely cited past sequences, (4) there have been sizable shifts in $T_{\rm eff}$s reported for some stars (especially among the hottest and coolest dwarf stars) over the past few decades, and (5) there have been subtle changes to the dwarf spectral sequence over the decades, especially among the M dwarfs. In light of the subtle shifts of the MK system over the past decades, improvements in the modeling of stellar atmospheres, and given the large volume of optical–IR photometry and derived stellar parameters in the literature now, a reevaluation of the temperature and colors scales is overdue.

We present our modern intrinsic color–$T_{\rm eff}$–spectral type tabulation for dwarfs in Table 5. This color tabulation was independently derived, and is *not* dependent on previous compendia of dwarf photometric properties. There were several stages that went into assembling Table 5. When discussing samples of "nearby stars," we assumed that stars with trigonometric parallax distances within 75 pc had negligible reddening (e.g., Reis et al. 2011), and so could be used to estimate intrinsic colors. While we often quote the intrinsic stellar colors to 0.001 mag precision (to ensure construction of smooth sequences on color–color plots), the uncertainty in the mean colors is typically at the ∼0.01 mag level, but can be upward of a few hundredths of a magnitude for the M-type dwarfs (where the uncertainties reflect differences among the colors of the standard stars themselves, and in the mean colors for stars of a given subtype). The first step was to estimate the mean intrinsic colors for each dwarf spectral subtype among one or more colors sensitive to spectral type, using both standard stars and samples of field stars with subtypes measured by expert classifiers. To anchor spectral type to these colors sensitive to spectral type, we used dereddened $U-B$ colors for OB dwarf stars, $B-V$ colors for AFGK dwarfs, and $V - K_s$ colors for M dwarfs.

C.1. Spectral Standard Stars

Spectral standard stars for stars of F-type and earlier were mostly drawn from Johnson & Morgan (1953), Morgan & Hiltner (1965), Garrison (1967), Lesh (1968), Abt et al. (1968), Hiltner et al. (1969), Cowley et al. (1969), Garrison (1972), Cowley (1972), Morgan & Keenan (1973), Cowley & Fraquelli (1974), Houk & Cowley (1975), Garrison et al. (1977), Morgan et al. (1978), Garrison & Schild (1979), Gray & Garrison (1987), Walborn & Fitzpatrick (1990), Garrison & Gray (1994), Garrison (1994), and Gray & Corbally (2009). For M-type stars,

the primary sources of standard stars were Kirkpatrick et al. (1991, 1997) and Henry et al. (2002). Some M-type standards from Keenan's papers (e.g., Keenan & McNeil 1976; Keenan & Pitts 1980; Keenan 1983; Keenan & Yorka 1988; Keenan & McNeil 1989) that have conflicting types compared to the newer classifications by Kirkpatrick, Henry, and collaborators, have been deprecated (e.g., GJ 15A, 172, 250B, 526) and were not considered in assessing median colors and $T_{\rm eff}$. Given the immense volume of recent M-star classifications that have been done on the Kirkpatrick & Henry grid (e.g., Reid et al. 1995; Hawley et al. 1996; Henry et al. 2002), these should be preferred to the Keenan types where there is disagreement. Classifications of AFGK field dwarfs by Gray et al. (2003, 2006) were generally preferred over those of the Michigan Atlas (Houk & Cowley 1975), as it appears that the Gray et al. classifications more closely follow the Morgan–Keenan standards. Differences between Gray et al. and Houk et al. classifications are especially pronounced amongst the early G-type stars. Part of this may stem from disagreement between Morgan and Keenan on the F/G boundary (e.g., see the example of η Cas A previously mentioned). More problematically, Houk & Cowley (1975) considered β Com to be their main G2V standard, but it was considered to be a G0V standard by Johnson & Morgan (1953), Morgan et al. (1971), Morgan & Keenan (1973), and Keenan & McNeil (1976). This appears to explain why the median $B-V$ color for nearby G2V stars in the Hipparcos catalog (dominated by Michigan Atlas classifications) is $B-V \simeq 0.617$, whereas for stars classified G2V by Gray et al. (2001b, 2003, 2006) on Keenan's standard star grid, $B-V \simeq 0.647$ (remarkably similar to the recent precise estimate of the solar $B-V$ color of 0.653 ± 0.003 by Ramírez et al. 2012). As Keenan's G/K-type standard stars are in common usage, we weight the median colors for field dwarfs classified using the Keenan standards (e.g., Gray's papers) over those from the Michigan Atlases (e.g., Houk & Cowley 1975).

C.2. Assessing the Pedigree of Spectral Standard Stars

An extensive literature search was conducted to assemble notes on the published classifications and colors for *all* known O- through M-type dwarf spectral type standard stars (The notes have been compiled at http://www.pas.rochester.edu/~emamajek/spt/ and will be periodically updated as needed). All the dwarf spectral standards were assessed for continuity in their spectral classifications over the decades, and standards were graded as "anchor standards" (Garrison 1994), "primary standards," "secondary standards," "tertiary standards," "variant standards," or "deprecated standards." Our terminology is a variation on the hierarchy scheme of Garrison (1994), and the goal of assessing the pedigree of the various spectral standards was to help in the estimation of the best stellar parameters reflective of a given spectral subtype. While the grading of the individual standards is not provided here, the reader is referred to the Web site mentioned. "Anchor standards" are those rare standard stars listed by Garrison (1994) whose spectral types have remained unchanged since Morgan et al. (1943), and which essentially define the MK system. "Primary standards" typically showed very strong continuity in adopted spectral types among expert classifiers, often going back to Johnson & Morgan (1953). "Secondary standards" usually appeared several times in the literature as spectral standards, but sometimes expert classifiers assigned slightly different spectral types to the star (usually at the $\pm$0.5–2 subtypes level). "Tertiary standards" were rarely graded as such, but this was usually the category assigned when the standard was only considered as such by one study, and with no or few dissensions or corroborating classifications, e.g., the B8V standard HR 9050 (considered only a standard by Garrison & Gray 1994). "Variant standards" are standards with spectral peculiarities (usually demonstrating very non-solar composition), e.g., the G5Vb Fe-2 star 85 Peg (Keenan & Yorka 1988), and these were ignored when considering adopted subtype colors. As Garrison (1994) discussed, the "anchor standards" are those that have remained unchanged since Morgan et al. (1943), and essentially define the backbone of the MK system. Occasionally, a star whose classification has varied over the years is considered a primary standard only because no better standard is available (e.g., 16 Cyg B, a "primary" G3V standard, but whose classifications have varied from G2V to G5V over the years; Keenan & McNeil 1976, 1989; Gray et al. 2001b). "Deprecated standards" were considered those standard stars whose spectral types determined by expert classifiers had changed appreciably over the years (even by the same classifier!), while higher pedigree standards for that subtype were available. An example of a deprecated standard is η Cas A, considered an F9V standard by Keenan & Yorka (1988), Keenan & McNeil (1989), and Gray et al. (2001b), but considered a G0V standard by Morgan et al. (1943), Johnson & Morgan (1953), Morgan & Keenan (1973), Keenan & McNeil (1976), Morgan et al. (1978), Keenan (1983), and Keenan & Yorks (1985). Another example is σ Boo (HR 5447), which was considered a F2V standard by Morgan et al. (1943) and Johnson & Morgan (1953), but two later studies found the star to appear spectrally metal poor (F3V vw; Barry 1970 and F4V kF2 mF1; Gray et al. 2001b). Use of such standards should probably be avoided in the future, if possible.

While estimating the parameters for a given dwarf spectral subtype, more weight was assigned to the individual parameters (e.g., colors, $T_{\rm eff}$s) of the anchor and primary standards compared to the secondary and tertiary standards, and the properties of the variant and deprecated standards were largely ignored. While estimating the typical properties of non-standard stars of a given spectral subtype, we employed median values throughout, in order to avoid the effects of interloper data (Gott et al. 2001). The properties of both standard and non-standard stars were incorporated into estimation of typical colors and $T_{\rm eff}$s, and their properties usually agreed well with very few exceptions (e.g., B7V, where the lone good standard star HD 21071 appears to be significantly bluer and hotter than the majority of field stars classified B7V).

C.3. Color Sequences

The intrinsic $(B-V)_o$ and $(U-B)_o$ colors can be derived for OB dwarfs via the Q-method (e.g., Johnson & Morgan 1953; Johnson 1958; Hiltner & Johnson 1956), where the reddening-free index Q is calculated using the observed colors as $Q = (U-B) - 0.72(B-V)$. Functions of $(B-V)_o$ and $(U-B)_o$ as linear functions of Q, especially those that are forced through the origin ($(B-V)_o$, $(U-B)_o$), produce poor fits to the colors of real unreddened OB stars. We calibrated new Q versus intrinsic color relations using UBV photometry from Mermilliod & Mermilliod (1994) of nearby negligibly reddened B-type dwarfs within 75 pc (*Hipparcos* catalog; ESA 1997), and lightly reddened hotter O- and early-B luminosity class V and IV stars in nearby associations. The more distant OB stars were dereddened using published H I column densities (e.g., Fruscione et al. 1994) and the strong correlation between N(H I) and $E(B-V)$; Diplas & Savage (1994). The improved

Q-method fits are:

$$(B-V)_o = -4.776008156728 \times 10^{-3} + 0.5522012574154\,Q + 1.151583004497\,Q^2 + 1.829921229667\,Q^3 + 0.8933113140506\,Q^4$$

for $-0.32 < (B-V)_o < 0.02$, and

$$(U-B)_o = 6.230566666312 \times 10^{-3} + 1.533217755592\,Q + 1.385407188924\,Q^2 + 2.167355580182\,Q^3 + 1.075207514655\,Q^4$$

for $-1.13 < (U-B)_o < 0.02$. We find that the intrinsic $(B-V)_o$ colors of O9/B0 dwarfs are -0.32 to -0.31 (among the calibrator stars e.g., 10 Lac, σ Sco, τ Sco, and υ Ori), in agreement with Johnson's classic work (e.g., Johnson & Morgan 1953; Johnson 1966, but at odds with the recent work of Martins & Plez (2006) who claim that $(B-V)_o$ colors of Galactic O stars go no bluer than -0.28.

Deriving the MS color sequence was fairly straightforward. Photometry for nearby stars came from the following sources: *UBV* Mermilliod (1991), BVI_C (ESA 1997), JHK_S (Skrutskie et al. 2006), $W1$, $W2$, $W3$, and $W4$ (Cutri & et al. 2012). While we did derive median color estimates for each type (some are listed in the individual spectral type files), we decided to fit polynomials to the color–color data for nearby field dwarfs. For some color–color sequences polynomials give inadequate fits. For these instances we found it more reliable to simply construct a well-sampled color–color table based on median colors within a given color bin, and interpolate (e.g., $V-K_S$ versus $B-V$, $V-I_C$, $J-H$, $H-K_S$, $B-V$ versus $V-I_C$ and $U-B$). We fit polynomial relations to $V-K_S$ versus K_S-W1, K_S-W2, K_S-W3, and K_S-W4 for stars within 75 pc from the *Hipparcos* catalog and the catalog of bright M dwarfs from Lépine & Gaidos (2011). We adopted V magnitudes from the APASS Data Release 6 catalog (Henden et al. 2012) for objects not present in the *Hipparcos* catalog, and only fit objects with high quality photometry in the relevant band (for 2MASS bands, quality flag "A"; for *WISE* bands, contamination and confusion flag "0"). We restricted the data to *WISE* magnitudes $W1 > 5.0$, $W2 > 6.0$, $W3 > 5.0$ and $W4 > 0.0$ to avoid biases due to saturation. The data is not well-populated for $V-K_S < 0.5$ mag or $V-K_S > 6.0$ mag, so Table 5 only contains *WISE* colors for spectral types F0 through M5.

C.4. Effective Temperatures

Subtype $T_{\rm eff}$s were estimated by considering published $T_{\rm eff}$s for individual stars of a given subtype, though greater weighting was given to $T_{\rm eff}$ values for spectral standards which were vetted for consistent classifications in the literature. Our search for published $T_{\rm eff}$s was extensive, though not exhaustive, and given time constraints we are admittedly limited by what values were published in electronic tables that could be easily queried with e.g., Vizier.[13] Many $T_{\rm eff}$s came from large catalogs by, e.g., Philip & Egret (1980), Sokolov (1995), Cayrel de Strobel et al. (1997), Blackwell & Lynas-Gray (1998), Gray et al. (2001a), Gray et al. (2003), Taylor (2005), Valenti & Fischer (2005), Paunzen et al. (2006), Gerbaldi et al. (2007), Fitzpatrick & Massa (2007), Prugniel et al. (2007), Zorec et al. (2009), Soubiran et al. (2010), and Casagrande et al. (2011), and the authors calculated photometric $T_{\rm eff}$s for OB dwarf standards using photometry from Hauck & Mermilliod (1998), dereddening relations from Castelli (1991), and color–temperature relations from Balona & Shobbrook (1984), Napiwotzki et al. (1993), and Balona (1994). $T_{\rm eff}$s were also estimated for OB dwarf standards using $U-B$ versus $T_{\rm eff}$ data in Bessell et al. (1998).

Here is an example of our evaluation of the median $T_{\rm eff}$ for A0V stars. We find very consistent effective temperatures among A0V standards within a few hundred K of each other. The A0V standard Vega has had a very precise apparent $T_{\rm eff}$ measured by Monnier et al. (2012) of 9660 K (in good agreement with many previous estimates), and we find the literature median $T_{\rm eff}$ for the other widely used MK standards γ UMa and HR 3314 to be 9361 K and 9760 K. While there are other A0V standards, two of these (γ UMa, Vega) are considered "anchor" standards by Garrison (1994) (i.e., their classifications have remained the same over seven decades of use), and HR 3314 has retained its A0V standard status throughout (Morgan et al. 1953; Johnson & Morgan 1953; Garrison & Schild 1979; Gray & Garrison 1987; Houk & Swift 1999; Gray et al. 2003). An exhaustive search for $T_{\rm eff}$s for A0V stars in the literature (265 estimates) yields a median $T_{\rm eff}$ of 9707 K. Based on these values, we adopt a median $T_{\rm eff}$ of 9700 K for A0V stars. We find it unlikely that the median A0V $T_{\rm eff}$ could be as high as 10000 K (Bessell 1979; Crowther 1997), nor as low as 9394 K (Boyajian et al. 2012a), 9520 K (Schmidt-Kaler 1982), or 9530 K (Theodossiou & Danezis 1991). We note in particular that the recently published $T_{\rm eff}$ scale by Boyajian et al. (2012a) appears to be most deviant among the A0V $T_{\rm eff}$ values, and while that study relies on new interferometric observations, their survey contained only a single non-standard A0V star (HD 177724). Similarly sized deviations at the hundreds of K level were seen between our $T_{\rm eff}$ scale and the Boyajian et al. (2012a) $T_{\rm eff}$ scale. So while there are other modern color/$T_{\rm eff}$ scales in the literature, we believe that ours is based on a very broad (but vetted) amount of photometric/$T_{\rm eff}$ literature and classifications.

C.5. Bolometric Corrections

The BCs listed in Table 5 are derived for each spectral type by adopting the median BC among several scales as a function of the adopted $T_{\rm eff}$, including Balona (1994), Bertone et al. (2004), Flower (1996), Bessell et al. (1998), Masana et al. (2006), Schmidt-Kaler (1982), Code et al. (1976), Casagrande et al. (2006, 2008, 2010), Lanz & Hubeny (2007), Vacca et al. (1996), and Lanz & Hubeny (2003)[14] where they applicable. For the M dwarfs, the BC_V scale was estimated via $V-K_s$ colors and the BC_K results from Leggett et al. (2001), Dahn et al. (2002), and Golimowski et al. (2004), as well as the authors' SEDF fits compiled in Table 7.

REFERENCES

Abt, H. A., Meinel, A. B., Morgan, W. W., & Tapscott, I. W. 1968, An Atlas of Low-dispersion Grating Stellar Spectra (Tucson, AZ: Kitt Peak National Observatory)
Allard, F., Homeier, D., & Freytag, B. 2012, RSPTA, 370, 2765
Allen, L. E., & Strom, K. M. 1995, AJ, 109, 1379
Alonso, A., Arribas, S., & Martínez-Roger, C. 1999, A&AS, 140, 261
Asplund, M., Grevesse, N., Sauval, A. J., & Scott, P. 2009, ARA&A, 47, 481
Bailey, J. I., III, White, R. J., Blake, C. H., et al. 2012, ApJ, 749, 16

[13] http://vizier.u-strasbg.fr/viz-bin/VizieR

[14] Extensive notes and discussion can be found for each spectral type at http://www.pas.rochester.edu/~emamajek/spt/.

Balona, L. A. 1994, MNRAS, 268, 119
Balona, L. A., & Shobbrook, R. R. 1984, MNRAS, 211, 375
Baraffe, I., Chabrier, G., Allard, F., & Hauschildt, P. H. 1998, A&A, 337, 403
Barnes, T. G., & Evans, D. S. 1976, MNRAS, 174, 489
Barrado Y Navascués, D. 2006, A&A, 459, 511
Barry, D. C. 1970, ApJS, 19, 281
Bell, C. P. M., Naylor, T., Mayne, N. J., Jeffries, R. D., & Littlefair, S. P. 2012, MNRAS, 424, 3178
Bell, C. P. M., Naylor, T., Mayne, N. J., Jeffries, R. D., & Littlefair, S. P. 2013, arXiv:1306.3237
Bertone, E., Buzzoni, A., Chávez, M., & Rodríguez-Merino, L. H. 2004, AJ, 128, 829
Bessell, M., & Murphy, S. 2012, PASP, 124, 140
Bessell, M. S. 1979, PASP, 91, 589
Bessell, M. S., & Brett, J. M. 1988, PASP, 100, 1134
Bessell, M. S., Castelli, F., & Plez, B. 1998, A&A, 333, 231
Blackwell, D. E., & Lynas-Gray, A. E. 1998, A&AS, 129, 505
Blackwell, D. E., & Shallis, M. J. 1977, MNRAS, 180, 177
Boyajian, T. S., McAlister, H. A., van Belle, G., et al. 2012a, ApJ, 746, 101
Boyajian, T. S., von Braun, K., van Belle, G., et al. 2012b, ApJ, 757, 112
Cannon, A. J., & Pickering, E. C. 1918, AnHar, 91, 1
Carpenter, J. M. 2001, AJ, 121, 2851
Casagrande, L., Flynn, C., & Bessell, M. 2008, MNRAS, 389, 585
Casagrande, L., Portinari, L., & Flynn, C. 2006, MNRAS, 373, 13
Casagrande, L., Ramírez, I., Meléndez, J., & Asplund, M. 2012, ApJ, 761, 16
Casagrande, L., Ramírez, I., Meléndez, J., Bessell, M., & Asplund, M. 2010, A&A, 512, A54
Casagrande, L., Schönrich, R., Asplund, M., et al. 2011, A&A, 530, A138
Castelli, F. 1991, A&A, 251, 106
Castelli, F., & Kurucz, R. L. 2004, arXiv:astro-ph/0405087
Cayrel de Strobel, G., Soubiran, C., Friel, E. D., Ralite, N., & Francois, P. 1997, A&AS, 124, 299
Code, A. D., Bless, R. C., Davis, J., & Brown, R. H. 1976, ApJ, 203, 417
Cowley, A. 1972, AJ, 77, 750
Cowley, A., Cowley, C., Jaschek, M., & Jaschek, C. 1969, AJ, 74, 375
Cowley, A., & Fraquelli, D. 1974, PASP, 86, 70
Cox, D. P., & Reynolds, R. J. 1987, ARA&A, 25, 303
Crowther, P. A. 1997, in IAU Symp. 189, The Effective Temperatures of Hot Stars, ed. T. R. Bedding, A. J. Booth, & J. Davis (Cambridge: Cambridge Univ. Press), 137
Cutri, R. M., et al. 2012, yCat, 2311, 0
Cutri, R. M., Skrutskie, M. F., van Dyk, S., et al. 2003, yCat, 2246, 0
Da Rio, N., Robberto, M., Soderblom, D. R., et al. 2010, ApJ, 722, 1092
Dahn, C. C., Harris, H. C., Vrba, F. J., et al. 2002, AJ, 124, 1170
de la Reza, R., Torres, C. A. O., Quast, G., Castilho, B. V., & Vieira, G. L. 1989, ApJL, 343, L61
Diplas, A., & Savage, B. D. 1994, ApJ, 427, 274
Engelke, C. W., Price, S. D., & Kraemer, K. E. 2010, AJ, 140, 1919
Epchtein, N., de Batz, B., Capoani, L., et al. 1997, Msngr, 87, 27
ESA. 1997, yCat, 1239, 0
Fitzpatrick, E. L., & Massa, D. 2007, ApJ, 663, 320
Flower, P. J. 1996, ApJ, 469, 355
Fruscione, A., Hawkins, I., Jelinsky, P., & Wiercigroch, A. 1994, ApJS, 94, 127
Garrison, R. F. 1967, ApJ, 147, 1003
Garrison, R. F. 1972, ApJ, 177, 653
Garrison, R. F. 1994, in ASP Conf. Ser. 60, The MK Process at 50 Years: a Powerful Tool for Astrophysical Insight, ed. C. J. Corbally, R. O. Gray, & R. F. Garrison (San Francisco, CA: ASP), 3
Garrison, R. F., & Gray, R. O. 1994, AJ, 107, 1556
Garrison, R. F., Hiltner, W. A., & Schild, R. E. 1977, ApJS, 35, 111
Garrison, R. F., & Schild, R. E. 1979, AJ, 84, 1020
Gáspár, A., Rieke, G. H., Su, K. Y. L., et al. 2009, ApJ, 697, 1578
Gautier, T. N., III, Rebull, L. M., Stapelfeldt, K. R., & Mainzer, A. 2008, ApJ, 683, 813
Gerbaldi, M., Faraggiana, R., & Caffau, E. 2007, A&A, 472, 241
Golimowski, D. A., Leggett, S. K., Marley, M. S., et al. 2004, AJ, 127, 3516
Gott, J. R., III, Vogeley, M. S., Podariu, S., & Ratra, B. 2001, ApJ, 549, 1
Gray, R. O. 1989, AJ, 98, 1049
Gray, R. O., & Corbally, J. C. (ed.) 2009, Stellar Spectral Classification (Princeton, NJ: Princeton Univ. Press)
Gray, R. O., Corbally, C. J., Garrison, R. F., et al. 2006, AJ, 132, 161
Gray, R. O., Corbally, C. J., Garrison, R. F., McFadden, M. T., & Robinson, P. E. 2003, AJ, 126, 2048
Gray, R. O., & Garrison, R. F. 1987, ApJS, 65, 581
Gray, R. O., Graham, P. W., & Hoyt, S. R. 2001a, AJ, 121, 2159
Gray, R. O., Napier, M. G., & Winkler, L. I. 2001b, AJ, 121, 2148
Grevesse, N., & Sauval, A. J. 1998, SSRv, 85, 161
Gullbring, E., Hartmann, L., Briceno, C., & Calvet, N. 1998, ApJ, 492, 323
Haberreiter, M., Schmutz, W., & Kosovichev, A. G. 2008, ApJL, 675, L53
Harlan, E. A. 1969, AJ, 74, 916
Hauck, B., & Mermilliod, M. 1998, A&AS, 129, 431
Hauschildt, P. H., Allard, F., & Baron, E. 1999, ApJ, 512, 377
Hauschildt, P. H., Baron, E., & Allard, F. 1997, ApJ, 483, 390
Hawley, S. L., Gizis, J. E., & Reid, I. N. 1996, AJ, 112, 2799
Henden, A. A., Levine, S. E., Terrell, D., Smith, T. C., & Welch, D. 2012, JAVSO, 40, 430
Henry, T. J., Walkowicz, L. M., Barto, T. C., & Golimowski, D. A. 2002, AJ, 123, 2002
Hiltner, W. A., Garrison, R. F., & Schild, R. E. 1969, ApJ, 157, 313
Hiltner, W. A., & Johnson, H. L. 1956, ApJ, 124, 367
Hoff, W., Henning, T., & Pfau, W. 1998, A&A, 336, 242
Høg, E., Fabricius, C., Makarov, V. V., et al. 2000, A&A, 355, L27
Houk, N. (ed.) 1978, Michigan Catalogue of Two-dimensional Spectral Types for the HD Stars (Ann Arbor, MI: Univ. Michigan)
Houk, N., & Cowley, A. P. (ed.) 1975, University of Michigan Catalogue of Two-dimensional Spectral Types for the HD Stars, Vol. I (Ann Arbor, MI: Univ. Michigan)
Houk, N., & Smith-Moore, M. (ed.) 1988, Michigan Catalogue of Two-dimensional Spectral Types for the HD Stars, Vol. 4 (Ann Arbor, MI: Univ. Michigan)
Houk, N., & Swift, C. (ed.) 1999, Michigan Catalogue of Two-dimensional Spectral Types for the HD Stars, Vol. 5 (Ann Arbor, MI: Univ. Michigan)
Hutchinson, M. G., Evans, A., Winkler, H., & Spencer Jones, J. 1990, A&A, 234, 230
Jarrett, T. H., Cohen, M., Masci, F., et al. 2011, ApJ, 735, 112
Jeffries, R. D. 1995, MNRAS, 273, 559
Johnson, H. L. 1958, LowOB, 4, 37
Johnson, H. L. 1966, ARA&A, 4, 193
Johnson, H. L., & Morgan, W. W. 1953, ApJ, 117, 313
Jorgensen, U. G. 1996, in IAU Symp. 178, Molecules in Astrophysics: Probes & Processes, ed. E. F. van Dishoeck (Cambridge: Cambridge Univ. Press), 441
Kastner, J. H., Zuckerman, B., & Bessell, M. 2008, A&A, 491, 829
Keenan, P. C. 1983, BICDS, 24, 19
Keenan, P. C. 1984, in The MK Process and Stellar Classification, ed. R. F. Garrison (Toronto: Univ. of Toronto), 29
Keenan, P. C., & McNeil, R. C. 1976, An Atlas of Spectra of the Cooler Stars: Types G, K, M, S, and C. Part 1: Introduction and Tables (Columbus, OH: Ohio State Univ. Press)
Keenan, P. C., & McNeil, R. C. 1989, ApJS, 71, 245
Keenan, P. C., & Pitts, R. E. 1980, ApJS, 42, 541
Keenan, P. C., & Yorka, S. B. 1988, BICDS, 35, 37
Keenan, P. C., & Yorks, S. B. 1985, BICDS, 29, 25
Kenyon, S. J., & Hartmann, L. 1995, ApJS, 101, 117
Kirkpatrick, J. D., Beichman, C. A., & Skrutskie, M. F. 1997, ApJ, 476, 311
Kirkpatrick, J. D., Henry, T. J., & McCarthy, D. W., Jr. 1991, ApJS, 77, 417
Kiss, L. L., Moór, A., Szalai, T., et al. 2011, MNRAS, 411, 117
Koen, C., Kilkenny, D., van Wyk, F., & Marang, F. 2010, MNRAS, 403, 1949
Kupka, F., Piskunov, N., Ryabchikova, T. A., Stempels, H. C., & Weiss, W. W. 1999, A&AS, 138, 119
Lafrasse, S., Mella, G., Bonneau, D., et al. 2010, Proc. SPIE, 7734, 77344E
Lanz, T., & Hubeny, I. 2003, ApJS, 146, 417
Lanz, T., & Hubeny, I. 2007, ApJS, 169, 83
Lawson, W. A., Crause, L. A., Mamajek, E. E., & Feigelson, E. D. 2001, MNRAS, 321, 57
Lawson, W. A., Crause, L. A., Mamajek, E. E., & Feigelson, E. D. 2002, MNRAS, 329, L29
Leggett, S. K., Allard, F., Geballe, T. R., Hauschildt, P. H., & Schweitzer, A. 2001, ApJ, 548, 908
Lépine, S., & Gaidos, E. 2011, AJ, 142, 138
Lépine, S., & Simon, M. 2009, AJ, 137, 3632
Lesh, J. R. 1968, ApJS, 17, 371
Looper, D. L., Bochanski, J. J., Burgasser, A. J., et al. 2010a, AJ, 140, 1486
Looper, D. L., Burgasser, A. J., Kirkpatrick, J. D., & Swift, B. J. 2007, ApJL, 669, L97
Looper, D. L., Mohanty, S., Bochanski, J. J., et al. 2010b, ApJ, 714, 45
Luhman, K. L. 1999, ApJ, 525, 466
Luhman, K. L., Allen, P. R., Espaillat, C., Hartmann, L., & Calvet, N. 2010a, ApJS, 189, 353
Luhman, K. L., Allen, P. R., Espaillat, C., Hartmann, L., & Calvet, N. 2010b, ApJS, 186, 111
Luhman, K. L., Stauffer, J. R., Muench, A. A., et al. 2003, ApJ, 593, 1093
Luhman, K. L., & Steeghs, D. 2004, ApJ, 609, 917

Lyo, A.-R., Lawson, W. A., Feigelson, E. D., & Crause, L. A. 2004, MNRAS, 347, 246
Mamajek, E. E. 2005, ApJ, 634, 1385
Mamajek, E. E. 2009, in AIP Conf. Ser. 1158, Exoplanets and Disks: Their Formation and Diversity, ed. T. Usuda, M. Tamura, & M. Ishii (Melville, NY: AIP), 3
Mamajek, E. E. 2012, ApJL, 754, L20
Mamajek, E. E., Lawson, W. A., & Feigelson, E. D. 1999, ApJL, 516, L77
Mamajek, E. E., Meyer, M. R., & Liebert, J. 2002, AJ, 124, 1670
Mamajek, E. E., Meyer, M. R., & Liebert, J. 2006, AJ, 131, 2360
Martins, F., & Plez, B. 2006, A&A, 457, 637
Masana, E., Jordi, C., & Ribas, I. 2006, A&A, 450, 735
McCarthy, K. A., & White, R. J. 2012, AJ, 143, 134
Megeath, S. T., Hartmann, L., Luhman, K. L., & Fazio, G. G. 2005, ApJL, 634, L113
Mentuch, E., Brandeker, A., van Kerkwijk, M. H., Jayawardhana, R., & Hauschildt, P. H. 2008, ApJ, 689, 1127
Mermilliod, J. C. 1991, Homogeneous Means in the UBV System (Lausanne: Institut d'Astronomie, Université de Lausanne)
Mermilliod, J.-C., & Mermilliod, M. (ed.) 1994, Catalogue of Mean UBV Data on Stars (Berlin: Springer)
Monnier, J. D., Che, X., Zhao, M., et al. 2012, ApJL, 761, L3
Morgan, W. W., Abt, H. A., & Tapscott, J. W. 1978, Revised MK Spectral Atlas for Stars Earlier Than the Sun
Morgan, W. W., Harris, D. L., & Johnson, H. L. 1953, ApJ, 118, 92
Morgan, W. W., & Hiltner, W. A. 1965, ApJ, 141, 177
Morgan, W. W., Hiltner, W. A., & Garrison, R. F. 1971, AJ, 76, 242
Morgan, W. W., & Keenan, P. C. 1973, ARA&A, 11, 29
Morgan, W. W., Keenan, P. C., & Kellman, E. 1943, An Atlas of Stellar Spectra, with an Outline of Spectral Classification (Chicago, IL: The Univ. of Chicago Press)
Napiwotzki, R., Schoenberner, D., & Wenske, V. 1993, A&A, 268, 653
Paunzen, E., Schnell, A., & Maitzen, H. M. 2006, A&A, 458, 293
Pecaut, M. J., Mamajek, E. E., & Bubar, E. J. 2012, ApJ, 746, 154
Perryman, M. A. C., & ESA, (ed.) 1997, ESA Special Publication, Vol. 1200, The Hipparcos and Tycho Catalogues. Astrometric and Photometric Star Catalogues Derived from the ESA Hipparcos Space Astrometry Mission (Noordwijk: ESA)
Philip, A. D., & Egret, D. 1980, A&AS, 40, 199
Prugniel, P., Soubiran, C., Koleva, M., & Le Borgne, D. 2007, arXiv: astro-ph/0703658
Ramírez, I., Michel, R., Sefako, R., et al. 2012, ApJ, 752, 5
Rebull, L. M., Stapelfeldt, K. R., Werner, M. W., et al. 2008, ApJ, 681, 1484
Reid, I. N., Hawley, S. L., & Gizis, J. E. 1995, AJ, 110, 1838
Reid, N. 2003, MNRAS, 342, 837
Reis, W., Corradi, W., de Avillez, M. A., & Santos, F. P. 2011, ApJ, 734, 8
Riaz, B., Gizis, J. E., & Harvin, J. 2006, AJ, 132, 866
Rice, E. L., Barman, T., Mclean, I. S., Prato, L., & Kirkpatrick, J. D. 2010a, ApJS, 186, 63
Rice, E. L., Faherty, J. K., & Cruz, K. L. 2010b, ApJL, 715, L165
Rieke, G. H., Blaylock, M., Decin, L., et al. 2008, AJ, 135, 2245
Robertson, T. H., & Hamilton, J. E. 1987, AJ, 93, 959
Rodriguez, D. R., Bessell, M. S., Zuckerman, B., & Kastner, J. H. 2011, ApJ, 727, 62
Savage, B. D., & Mathis, J. S. 1979, ARA&A, 17, 73
Scandariato, G., Da Rio, N., Robberto, M., Pagano, I., & Stassun, K. 2012, A&A, 545, A19
Schlieder, J. E., Lépine, S., Rice, E., et al. 2012a, AJ, 143, 114
Schlieder, J. E., Lépine, S., & Simon, M. 2010, AJ, 140, 119
Schlieder, J. E., Lépine, S., & Simon, M. 2012b, AJ, 143, 80
Schmidt-Kaler, T. 1982, in Landolt-Börnstein—Group VI Astronomy and Astrophysics, Vol. 2b, Stars and Star Clusters, ed. K. Schaifers & H. Voigt (Berlin: Springer), 451
Schneider, A., Melis, C., & Song, I. 2012a, ApJ, 754, 39
Schneider, A., Song, I., Melis, C., Zuckerman, B., & Bessell, M. 2012b, ApJ, 757, 163
Scholz, R.-D., McCaughrean, M. J., Zinnecker, H., & Lodieu, N. 2005, A&A, 430, L49
Shkolnik, E., Liu, M. C., & Reid, I. N. 2009, ApJ, 699, 649
Shkolnik, E. L., Liu, M. C., Reid, I. N., Dupuy, T., & Weinberger, A. J. 2011, ApJ, 727, 6
Sicilia-Aguilar, A., Bouwman, J., Juhász, A., et al. 2009, ApJ, 701, 1188
Simon, M., & Schaefer, G. H. 2011, ApJ, 743, 158
Skrutskie, M. F., Cutri, R. M., Stiening, R., et al. 2006, AJ, 131, 1163
Sokolov, N. A. 1995, A&AS, 110, 553
Song, I., Bessell, M. S., & Zuckerman, B. 2002, ApJL, 581, L43
Song, I., Zuckerman, B., & Bessell, M. S. 2004, ApJ, 600, 1016
Soubiran, C., Le Campion, J.-F., Cayrel de Strobel, G., & Caillo, A. 2010, A&A, 515, A111
Stauffer, J. R., Jones, B. F., Backman, D., et al. 2003, AJ, 126, 833
Stauffer, J. R., Schultz, G., & Kirkpatrick, J. D. 1998, ApJL, 499, L199
Stephenson, C. B. 1986, AJ, 91, 144
Stephenson, C. B., & Sanduleak, N. 1977, PW&SO, 2, 71
Stephenson, C. B., & Sanwal, N. B. 1969, AJ, 74, 689
Sterzik, M. F., Alcalá, J. M., Covino, E., & Petr, M. G. 1999, A&A, 346, L41
Strassmeier, K. G., & Rice, J. B. 2000, A&A, 360, 1019
Taylor, B. J. 2005, ApJS, 161, 444
Teixeira, R., Ducourant, C., Chauvin, G., et al. 2009, A&A, 503, 281
Teixeira, R., Ducourant, C., Chauvin, G., et al. 2008, A&A, 489, 825
Theodossiou, E., & Danezis, E. 1991, Ap&SS, 183, 91
Torres, C. A. O., Quast, G. R., da Silva, L., et al. 2006, A&A, 460, 695
Torres, G. 2010, AJ, 140, 1158
Torres-Dodgen, A. V., & Weaver, W. B. 1993, PASP, 105, 693
Vacca, W. D., Garmany, C. D., & Shull, J. M. 1996, ApJ, 460, 914
Vacca, W. D., & Sandell, G. 2011, ApJ, 732, 8
Valenti, J. A., & Fischer, D. A. 2005, ApJS, 159, 141
van Belle, G. T., Lane, B. F., Thompson, R. R., et al. 1999, AJ, 117, 521
van Leeuwen, F. 2007, A&A, 474, 653
Viana Almeida, P., Santos, N. C., Melo, C., et al. 2009, A&A, 501, 965
Vyssotsky, A. N. 1956, AJ, 61, 201
Walborn, N. R., & Fitzpatrick, E. L. 1990, PASP, 102, 379
Walter, F. M., Stringfellow, G. S., Sherry, W. H., & Field-Pollatou, A. 2004, AJ, 128, 1872
Weinberger, A. J., Anglada-Escudé, G., & Boss, A. P. 2013, ApJ, 762, 118
Weis, E. W. 1993, AJ, 105, 1962
White, R. J., & Hillenbrand, L. A. 2004, ApJ, 616, 998
Worthey, G., & Lee, H.-c. 2011, ApJS, 193, 1
Wright, E. L., Eisenhardt, P. R. M., Mainzer, A. K., et al. 2010, AJ, 140, 1868
Zorec, J., Cidale, L., Arias, M. L., et al. 2009, A&A, 501, 297
Zuckerman, B., Rhee, J. H., Song, I., & Bessell, M. S. 2011, ApJ, 732, 61
Zuckerman, B., & Song, I. 2004, ARA&A, 42, 685
Zuckerman, B., Song, I., Bessell, M. S., & Webb, R. A. 2001, ApJL, 562, L87